Research article

urn:lsid:zoobank.org:pub:6E985EF6-5434-40BA-92FA-3D7F710380B9

Unveiling an enigma from the Cerrado: taxonomic revision of two sympatric species of *Apostolepis* Cope, 1862 (Dipsadidae: Xenodontinae: Elapomorphini) from central Brazil

Omar M. ENTIAUSPE-NETO [1,*], Claudia KOCH [2], Thaís B. GUEDES [3],
Rafael C.B. PAREDERO [4], Arthur TIUTENKO [5] & Daniel LOEBMANN [6]

[1,4] Laboratório de Coleções Zoológicas, Instituto Butantan, 05503-90, Av. Vital Brazil, 1500, Butantã, São Paulo, SP, Brazil.
[1] Universidade Federal do Rio Grande do Sul, Instituto de Biociências, Departamento de Zoologia, Avenida Bento Gonçalves, CEP 91501-970, Porto Alegre, RS, Brazil.
[2] Zoologisches Forschungsmuseum Alexander Koenig, Adenauerallee 160, 53113, Bonn, Germany.
[3] Universidade Estadual do Maranhão, Centro de Estudos Superiores de Caxias, Praça Duque de Caxias, 65604-380, Caxias, MA, Brazil.
[3] Gothenburg Global Biodiversity Center, University of Gothenburg, Department of Biological and Environmental Sciences, Box 461, SE-405 30, Göteborg, Sweden.
[5] Friedrich-Alexander-Universität Erlangen-Nürnberg, Schloßplatz 4, 91054, Erlangen, Germany.
[6] Laboratório de Vertebrados Terrestres, Instituto de Ciências Biológicas, Universidade Federal do Rio Grande, Av. Itália, Km 8, 96201-900, Rio Grande, RS, Brazil.

[*] Corresponding author: omarentiauspe@hotmail.com
[2] Email: C.Koch@leibniz-zfmk.de
[3] Email: thaisbguedes@yahoo.com.br
[4] Email: rafaparadero@gmail.com
[5] Email: arthur.tiutenko@fau.de
[6] Email: pinguimfiel@yahoo.com.br

[1] urn:lsid:zoobank.org:author:C34B5FB1-0CAB-4AEC-9253-7CBDDCCEE9D9
[2] urn:lsid:zoobank.org:author:9B7ABFF8-8533-4563-A380-4637BA1A7FEF
[3] urn:lsid:zoobank.org:author:8491B33D-32C1-4C58-9A52-7627A7C5CAED
[4] urn:lsid:zoobank.org:author:A3E0289A-12AA-4548-BD7E-F379D0021EB1
[5] urn:lsid:zoobank.org:author:8AF2246D-B7CE-4140-BF4B-6A9B7568BB0F
[6] urn:lsid:zoobank.org:author:DC97B513-B045-4A34-9BF7-47024B71567F

Abstract. *Apostolepis albicollaris* and *A. cerradoensis* are two Elapomorphini snake species, described within a short timespan, from the Cerrado of central Brazil. In their brief descriptions, these two species were diagnosed from congeners largely based on highly variable external morphological characters. Interestingly enough, *A. cerradoensis* has remained known based on a single specimen since its description. Here, we present a reanalysis of both type specimens, as well as a careful examination of a large series of specimens formerly assigned to these species, based on the comparison of internal and external morphology. We conclude that both species are synonymous, providing evidence for the recognition of *A. cerradoensis* as a junior synonym of *A. albicollaris*. Furthermore, an account of its updated diagnosis,

morphological variation, geographic distribution, hemipenial morphology, phylogenetic relationships and an osteological description are also provided. We also discuss its conservation status, suggesting that the species is under threat and qualifies to be listed as Vulnerable (VU ab(iii)), considering its rarity, small geographic range, and persistent environmental threats.

Introduction

The Elapomorphini Jan, 1862 tribe is composed of five genera (*Apostolepis* Cope, 1862, *Coronelaps* Lema & Hofstadler-Deiques, 2010, *Elapomorphus* Wiegmann in Fitzinger, 1843, *Parapostolepis* Amaral, 1930, and *Phalotris* Cope, 1862), that include 51 species, distributed in most of cisandine South America (Ferrarezzi 1993; Entiauspe-Neto *et al*. 2019, 2021a). The species of these genera share reduced supralabial scalation (5–7), a second supralabial contacting the eye, a U-shaped frontoparietal suture, and a short dentigerous process of the dentary (Savitzky 1979; Ferrarezzi 1993, 1994; Zaher 1994, 1999; Zaher *et al*. 2009). The aforementioned genera are distinguished from each other based on characters of external (scalation, coloration) and internal (osteological, hemipenial) morphology, and have not yet been tested in a molecular phylogenetic framework (see Entiauspe-Neto *et al*. 2021b for an overview of generic diagnoses).

Of these, *Apostolepis* is the most speciose genus, with 35 species that range from central Colombia and the Guyana Shield, southwards into northern Argentina and southern Brazil (Entiauspe-Neto *et al*. 2020a, 2020c, 2021b). A considerable amount of this diversity can be found in Brazil, which harbors approximately 30 species, of which most are associated with the South American Dry Diagonal and other open landscapes (Rodrigues 1992; Giraudo & Scrocchi 1998; Lema 2003; Ferrarezzi *et al.* 2005; Curcio *et al.* 2011; Guedes *et al.* 2014a; Entiauspe-Neto *et al.* 2021b).

The taxonomy of *Apostolepis* has been historically unstable and confusing; several species of *Apostolepis* are known from less than 10 specimens, being poorly represented in scientific collections and seldom found in the field, which has likely contributed to its instability (Harvey 1999; Nogueira *et al.* 2012; Entiauspe-Neto *et al.* 2019). During the last decades, a considerable number of species of *Apostolepis* were described based on small series and subjective morphological diagnostic characters (e.g., Lema 2002, 2003, 2004a, 2004b; Lema & Renner 2011), which were later found to be synonymous with other congeners, as these diagnoses relied largely upon polymorphic characters (Ferrarezzi *et al.* 2005; Entiauspe-Neto *et al*. 2019, 2020a, 2020b, 2021a).

Lema (1993), in his work on the morphological variation of *Apostolepis dimidiata* Jan, 1863, proposed the synonymization of *A. barrioi* Lema, 1978 (later revalidated by the same author in Cabral *et al*. (2017)), *A. ventrimaculata* Lema, 1978, and *A. villaricae* Lema, 1978 with the former species, while also reporting on the extremes of morphological variation for the analyzed specimens. Some of the specimens reported by Lema (1993) that bore white nuchal collars were then reanalyzed by Lema (2002) and briefly described as *Apostolepis albicollaris* Lema, 2002, based solely on external morphology, with a holotype (MCP 8355) from "Parque Zoológico Distrito Federal", Brasília, Distrito Federal (mistakenly reported as the state of "Goiás" by the author), Brazil. Although only four specimens were part of the

type series of *A. albicollaris*, its description reported 27 additional specimens, from Distrito Federal, Goiás, and Minas Gerais, all from the Cerrado of Central Brazil.

Shortly after, Lema (2003) described another species of *Apostolepis* from the Central Brazil, *Apostolepis cerradoensis* Lema, 2003, known from a single specimen (reported by the author as UHESM 21800, now MCP 15219) from "Usina Hidrelétrica Serra da Mesa", Minaçu, in the Cerrado of Goiás, Brazil. Oddly enough, this species was compared exclusively to *A. dimidiata*, and also only briefly described based on external morphology. Until now, *A. cerradoensis* remains known only from its holotype (Nogueira *et al.* 2019). Nogueira *et al.* (2012) provided a redescription for *A. albicollaris*, with an account of its morphological variation, hemipenial morphology, and a key to some species of *Apostolepis* and species-groups; it should be noted that these authors did not analyze the type specimen of *A. cerradoensis*, and that the species is not mentioned in their work.

In this study, we review the taxonomic status of *A. albicollaris* and *A. cerradoensis*, reanalyzing and comparing both type specimens. Based on newly generated data from the types and additional *Apostolepis* specimens from the Cerrado of Central Brazil, we consider these species as synonymous, *A. cerradoensis* beign a junior synonym of *A. albicollaris*. We also provide an account of its updated diagnosis, morphological variation, geographic distribution, hemipenial morphology, phylogenetic relationships and an osteological description. We also discuss its conservation status, suggesting that the species is under threat and qualifies to be listed as Vulnerable (VU ab(iii)), considering its rarity, small geographic range, and persistent environmental threats.

Material and methods

We examined a total of 715 specimens of *Apostolepis* (Appendix 1, acronyms according to Sabaj (2019)), of which 437 belong to 19 species that range in the South American Dry Diagonal. Scale counts follow Dowling (1951) and Peters (1964), while sex determination was done with a ventral incision in the base of the tail. The emended diagnosis is based on the nomenclature used by Entiauspe-Neto *et al.* (2020a). We measured head length (from the center of the rostral to the corner of the mouth) and head width (at the corner of the mouth) to the nearest 0.01 mm using a dial caliper; snout-vent length (SVL, from the center of the rostral to the posterior margin of the cloacal scale) and tail length (TL, from the posterior margin of the cloacal scale to the distal tip of the terminal scale) to the nearest 1 mm using a flexible ruler. We measured scales on the right side of the head and defined our measurement within the description when appropriate. Data are summarized in Supplementary Table 1. We used the verified point record database of *A. albicollaris* (Supplementary Table 2) to map its distribution. We calculate its Extent of Occurrence (EOO) and Area of Occupancy (AOO; based on 2 km cell width) by using the Geospatial Conservation Assessment Tool (GeoCAT; Bachman *et al.* 2011). To better address the conservation status of the species, we included layers of land use and land cover changes (collection 4, year of 2019, MapBiomas 2021; Souza Jr *et al.* 2020), frequency of fire (collection 1, years between 2005 and 2015, MapBiomas 2021; Souza Jr *et al.* 2020), and protected areas (ICMBio 2021) while mapping. We constructed all maps on QGIS ver. 3.16 (QGIS Development Team 2021).

We used the environment R ver. 3.2.3 (R Core Team 2015) software for all statistical tests. We employed an Analysis of Variance (ANOVA) in order to assess group differentiation in meristic (ventrals, subcaudals) and morphometric (SVL, TL) characters for the male samples of *A. albicollaris* (n = 11) and *A. cerradoensis* (n = 1), while these two samples were compared for their pairwise mean values with Tukey's Range Test (Zar 1999). These comparative analyses could not be extended to females, as the single known specimen of *A. cerradoensis* is a male. We also evaluated the presence or absence of sexual dimorphism for the whole sample series with a *T*-test, after we evaluated the assumptions of univariate normality by using a Shapiro Wilk test, and homoscedasticity through Levene's test (Zar 1999). When

describing sexual dimorphism, we report ranges followed in parentheses by mean ± 1 standard deviation and sample size. For statistics, we provide samples of each group as subscripts.

We describe the skull morphology of the *A. albicollaris* (MCP 8355) and *A. cerradoensis* (MCP 15219) holotypes, based on high-resolution micro-CT scans, performed with a Bruker SkyScan 1173 at the MCP. The scans were recorded over a 180° rotation with a frame averaging of 2, an X-ray beam with 60 kV source voltage, 133 µA current, and an exposure time of 800 ms per projection, without the use of a filter. For the scan of *A. albicollaris* a rotation step of 0.2° degrees was used, resulting in 1200 projections, an isotropic voxel size of 7.08 µm, and a total scan duration of 49:17 min. For *A. cerradoensis* a rotation step of 0.23° degrees was used, resulting in 1043 projections, an isotropic voxel size of 8.51 µm, and a total scan duration of 55:47 min. We reconstructed the CT-datasets using N-Recon software ver. 1.7.1.6 (Bruker MicroCT) and rendered the images in three dimensions through the aid of Amira visualization software (FEI, Thermo Fisher Scientific). Segmentation to separate and color the bones was also performed using Amira. For the description of the skulls, we use the osteological terminology of Bullock & Tanner (1966) and Cundall & Irish (2008), and the description of the skulls follows Entiauspe-Neto *et al*. (2020a, 2021b). We compared the skulls of *A. albicollaris* and *A. cerradoensis* to descriptions of the skulls of *A. ambiniger*, *A. assimilis*, *A. cearensis* Gomes, 1915, and *A. sanctaeritae* (Ferrarezzi *et al*. 2005; Entiauspe-Neto *et al*. 2020a, 2021a, 2021b).

In order to evaluate genetic distances among species of *Apostolepis*, we selected available sequences at GenBank (NCBI), of *small unit ribosomal RNA* (*12S*) gene sequences (JQ598793–JQ598797, GQ457781, GQ457782) and *oocyte maturation factor* (*CMOS*) gene fragment sequences (JQ598965–JQ598969, GQ457843, GQ457844). Each gene fragment was aligned separately with the MUSCLE Alignment plugin (Edgar 2004), in Geneious Pro (Drummond *et al.* 2010) software, with default settings (Supplementary Files 1–4). For the protein-coding gene *CMOS*, we translated the alignment into proteins to check for sequence integrity and stop-codons. Uncorrected genetic distances (*p*-distances) were calculated using MEGA 11 (Tamura *et al.* 2011), for each gene separately, using a *d* parameter (Transitions + Transversions), while assuming uniform rates among sites and homogeneous pattern among lineages. The *p*-distance calculation was made based on the proportional (*p*) differences among nucleotide sites in which two compared sequences differ, as inferred through the division of nucleotide differences by the total number of nucleotides (Tamura *et al.* 2011).

In order to evaluate the phylogenetic relationships among *Apostolepis* taxa and verify phylogenetic information contained in the available sequences, in addition to the aforementioned gene fragments, we pooled available Caenophidian sequences of mtDNA [*12S, large unit ribosomal RNA* (*16S*), *cytochrome b* (*CYTB*), *NADH dehydrogenase subunit 2* (*ND2*), and *NADH dehydrogenase subunit 4* (*ND4*)] and nuDNA [*brain-derived neurotrophic factor* (*BDNF*), *CMOS, neurotrophin-3* (*NT3*), and *recombination activating gene 1* (*RAG1*)] gene fragments into a combined dataset (Supplementary Table 3). Each gene fragment was aligned separately with the MUSCLE Alignment plugin (Edgar 2004) in Geneious Pro ver. 7.1 (Drummond *et al.* 2010) software, with default settings, and then incorporated into a concatenated alignment (Supplementary File 5). In order to evaluate topological congruence, we employed inferences of Maximum Likelihood (ML) and Bayesian Inference (BI). In order to avoid topological effects of model-induced redundancy or overparameterization biases associated with the selection of substitution models, we employed separately two distinct models, namely the Hasegawa, Kishino, and Yano 1985 (HKY85, hereafter) model (Hasegawa *et al*. 1985), which only accounts for the rates of transitions and transversions and unequal base frequencies ($\pi A \neq \pi G \neq \pi C \neq \pi T$), and the General Time-Reversible model (Tavaré 1986; GTR, hereafter), which accounts for six substitution rate parameters and four equilibrium base frequency parameters, each applied with BI and ML analyses, respectively. A phylogenetic inference of ML was employed with RAxML ver. 7.2.8 (Stamatakis 2014), using the GTR+Γ model, and a Rapid Bootstrapping with search for best-scoring ML tree (*-f a*), using 100 bootstrap replicates

(Supplementary File 6). A phylogenetic inference of BI was also employed with MrBayes ver. 3.2.6 (Huelsenbeck & Ronquist 2001), using an HKY85 substitution model and Gamma rate variation parameter, with 1 100 000 Markov-Chain Monte Carlo chains, with a subsampling frequence of 200, a Burn-In Length of 100 000 and four heated chains; priors were set to unconstrained branch lengths, with a compound Dirichlet prior on branch lengths of (1, 01, 1, 1) and an exponential shape parameter (10). Resulting topologies of the Bayesian inference analysis were then analyzed for their consensus tree on TreeAnnotator, with a consensus support threshold arbitrarily defined (≥ 80 %) and pruned to contain Echinantherini Zaher, Grazziotin, Cadle, Murphy, Moura-Leite & Bonatto, 2009, Philodryadini Cope, 1886, Tachymenini Bailey, 1967, and Elapomorphini outgroups only (Supplementary File 7). The ML topology was then used to infer branch lengths and patristic distances (absolute time and mutation rate, to which patristic distances represent the sum of branch lengths used to link two species terminal nodes in a tree) as reinforcement proxies of genetic distance (Supplementary Table 4), following Montingelli *et al.* (2020) and Entiauspe-Neto *et al.* (2021c), inferred with the package Ape for R (R Core Team 2015; Paradis & Schliep 2019). For patristic distances, paraphyletic terminals were treated separately.

Results

Upon reanalysis of both type specimens, it became evident that the type of *A. cerradoensis* has a different voucher number than the one reported in its description; although reported as UHESM 21800 in Lema (2003: 125), it is here corrected to MCP 15219. The previous acronym seems to be a field number that actually refers to "Usina Hidrelétrica de Serra da Mesa", which refers to its type locality, rather than a scientific collection. According to Lema (2003: 126), *A. albicollaris* could be distinguished from *A. cerradoensis* (characters in parentheses) based on its black ventral coloration (white), fully black tail (white), and wider black lateral stripes (smaller). These coloration characters were previously shown to be highly variable in other Elapomorphini species (e.g., Entiauspe-Neto *et al.* 2019, 2020a, 2021a, 2021b). Another congener from the Cerrado, *Apostolepis dimidiata* Jan, 1862, has a remarkably wide variation in ventral and lateral stripe coloration, which ranges from uniformly cream venter and small lateral black stripes, to a fully black venter and dorsolateral area (Entiauspe-Neto *et al.* 2019, 2021a). Furthermore, no other specimens aside from the type are known for *A. cerradoensis*.

During our analyses of specimens formerly referred to as *A. albicollaris* or *A. cerradoensis*, we observed a near total overlap of morphological characters that are reportedly diagnostic for congeners (ventrals, subcaudals, supralabials, infralabials, SVL, and TL), as seen in Table 1. For our ANOVA analyses, we encountered no statistical differences for SVL ($F_{11,1} = 0.184$, $p < 0.7$, $n = 12$), as well as TL ($F_{11,1} = 0.115$, $p > 0.7$, $n = 12$), and subcaudal ($F_{11,1} = 0.331$, $p < 0.5$, $n = 12$) values. However, we did encounter differences among the ventrals ($F_{11,1} = 5.924$, $p < 0.03$, $n = 12$) of *A. albicollaris* and *A. cerradoensis*. Tukey's Range Test also recovered no differences for SVL ($p < 0.6$), TL ($p < 0.7$), of subcaudal ($p < 0.5$) values, encountering differences in ventral ($p < 0.05$) values. These differences in ventral scales can likely be attributed to sample size limitations, as there were only 11 males of *A. albicollaris* examined, and a single known specimen of *A. cerradoensis*.

Both species are also mentioned as sympatric (Lema 2003: 126), with several specimens of *A. albicollaris* being collected in Minaçu (type locality of *A. cerradoensis*), which further blurs any geographic distinction between both taxa. Considering the lack of diagnostic characters and large overlap of morphology, we conclude that both taxa are conspecific, considering *A. cerradoensis* as a junior synonym of *A. albicollaris*. We provide an updated account on the variation for this species below, as well as an updated emended diagnosis.

Table 1 (continued on next page). Summary of diagnostic characters for species of *Apostolepis* Cope, 1862 in the Cerrado of Central Brazil. Measurements are given in mm. Abbreviations: SVL = snout-vent length; TL = tail length; ♂ = male; ♀ = female.

	A. albicollaris	*A. assimilis*	*A. dimidiata*	*A. flavotorquata*	*A. goiasensis*	*A. intermedia*	*A. nelsonjorgei*	*A. sanctaeritae*
SVL	157–410	140–780	186–545	200–890	300–392	105–319	227–254	190–686
TL	17–50	10–55	15–43	18–50	30–40	13–40	39–43	18–64
Head color	Black	Black	Black	Blackish brown	Black	Black	Brown	Black
Light snout blotch	Present; small, divided, white	Present; undivided, large, white	Present; small, divided, white	Present or absent; small, divided, white	Present; small, divided, white	Present; small, divided, white	Present; small, divided	Present; large, orange
Supralabial blotch	Large, single, over 1st to 5th supralabials	Large, single, over 3rd to 5th supralabials	Large, single, over 1st to 5th supralabials	Medium, two, largest over 3rd to 5th supralabials	Large, single, over 2nd to 5th supralabials	Large, single, over 1st to 5th supralabials	Small, over 2nd to 4th supralabials	Medium, single, over 3rd and 4th supralabials
Light nuchal collar	Present, large (usually up to four rows)	Present, large (usually up to four rows)	Absent	Present, small (usually up to two rows)	Absent	Absent	Present, medium (usually up to three rows)	Present, two, large (usually up to five rows in first, three in second)
Black nuchal collar	Present, medium (usually up to three rows)	Present, medium (usually up to three rows)	Absent	Present, small (usually up to two rows)	Absent	Absent	Present, small (usually up to two rows)	Present, large (usually up to seven rows)
Gular color	Immaculate cream or black	Immaculate cream	Black	Immaculate cream	Immaculate cream	Black	Immaculate cream	Immaculate cream or black
Dorsal background color	Orange or red	Orange or red	Orange or red	Orange or red	Light orange or light red	Gray or light brown	Light brown	Orange
Dorsal stripes	Present, two black lateral stripes	Absent	Present, two black lateral stripes	Absent or present, three black stripes	Present, three brown stripes	Present, five black or brown stripes	Present, five brown stripes	Absent
Ventral color	Immaculate cream or black	Immaculate cream or orange	Immaculate cream or black	Yellow	Immaculate cream	Immaculate cream	Immaculate cream	Immaculate cream or orange
Tail black blotch	Present in dorsal and ventral view	Present in dorsal and ventral view	Present in dorsal and ventral view	Present in dorsal and ventral view	Present in dorsal and ventral view	Present in dorsal and ventral view	Present in dorsal and ventral view	Present in dorsal and ventral view

Table 1 (continued). Summary of diagnostic characters for species of *Apostolepis* Cope, 1862 in the Cerrado of Central Brazil. Measurements are given in mm.

	A. albicollaris	*A. assimilis*	*A. dimidiata*	*A. flavotorquata*	*A. goiasensis*	*A. intermedia*	*A. nelsonjorgei*	*A. sanctaeritae*
Terminal spine	Black or bicolor	Black	Black or bicolor	Black or bicolor	White or bicolor	White	Black	Black
Ventrals	196–208 (n = 13) ♂♂; 206–230 (n = 10) ♀♀	225–260 (n = 21) ♂♂; 243–268 (n = 22) ♀♀	226–240 (n = 6) ♂♂; 220–244 (n = 5) ♀♀	245–268 (n = 4) ♂♂; 229–250 (n = 5) ♀♀	214–223 (n = 2) ♂♂; 220–237 (n = 2) ♀♀	211–217 (n = 2) ♂♂; 230–242 (n = 2) ♀♀	234–244 (n = 2) ♂♂	219–240 (n = 12) ♂♂; 221–253 (n = 8) ♀♀
Subcaudals	24–33 (n = 13) ♂♂; 28–30 (n = 10) ♀♀	26–36 (n = 19) ♂♂; 24–31 (n = 19) ♀♀	25–28 (n = 6) ♂♂; 25–39 (n = 5) ♀♀	31–40 (n = 4) ♂♂; 26–33 (n = 5) ♀♀	27–33 (n = 2) ♂♂; 25–28 (n = 2) ♀♀	33–37 (n = 2) ♂♂; 28–38 (n = 2) ♀♀	49–52 (n = 2) ♂♂	32–36 (n = 8) ♂♂; 26–32 (n = 2) ♀♀
Supralabials	Six (rarely four, five, or seven)	Six (rarely five or seven)	Six	Six	Six or five	Six	Six or five	Six
Infralabials	Six or seven (rarely eight)	Six or seven	Seven	Seven	Seven	Six	Seven	Seven
Preocular-nasal contact	Present	Absent	Absent or present	Absent or present	Absent or present	Absent	Present	Absent
Tail tip	Rounded	Rounded or pointed	Rounded	Rounded	Pointed	Pointed	Pointed	Pointed
Hemipenes	Slightly bilobed, semicapitate, semicalyculate; body covered by moderately sized hooked spines on sulcate side, lamellae on capitulum	Slightly bilobed, almost simple and noncapitate, semicalyculate; body covered by moderately sized hooked spines on sulcate side	Slightly bilobed, capitate, semicalyculate; body covered by moderately sized hooked spines on sulcate side, lamellae on capitulum	Unilobed, simple, noncapitate, calyculate; spinules restricted to proximal area, enlarged spines absent, asulcate surface calyculate	Slightly bilobed, capitate, calyculate; body covered by moderately sized hooked spines on sulcate side, lamellae on capitulum	Unilobed, capitate, spinulate; body covered by spinules on sulcate side, hooked spines on asulcate side	–	Slightly bilobed, almost simple and noncapitate, semicalyculate; body covered by moderately sized hooked spines on sulcate side

Phylum Chordata Haeckel, 1874
Class Reptilia Laurenti, 1768
Order Squamata Oppel, 1811
Suborder Serpentes Linnaeus, 1758
Family Dipsadidae Bonaparte, 1838
Subfamily Xenodontinae Bonaparte, 1845
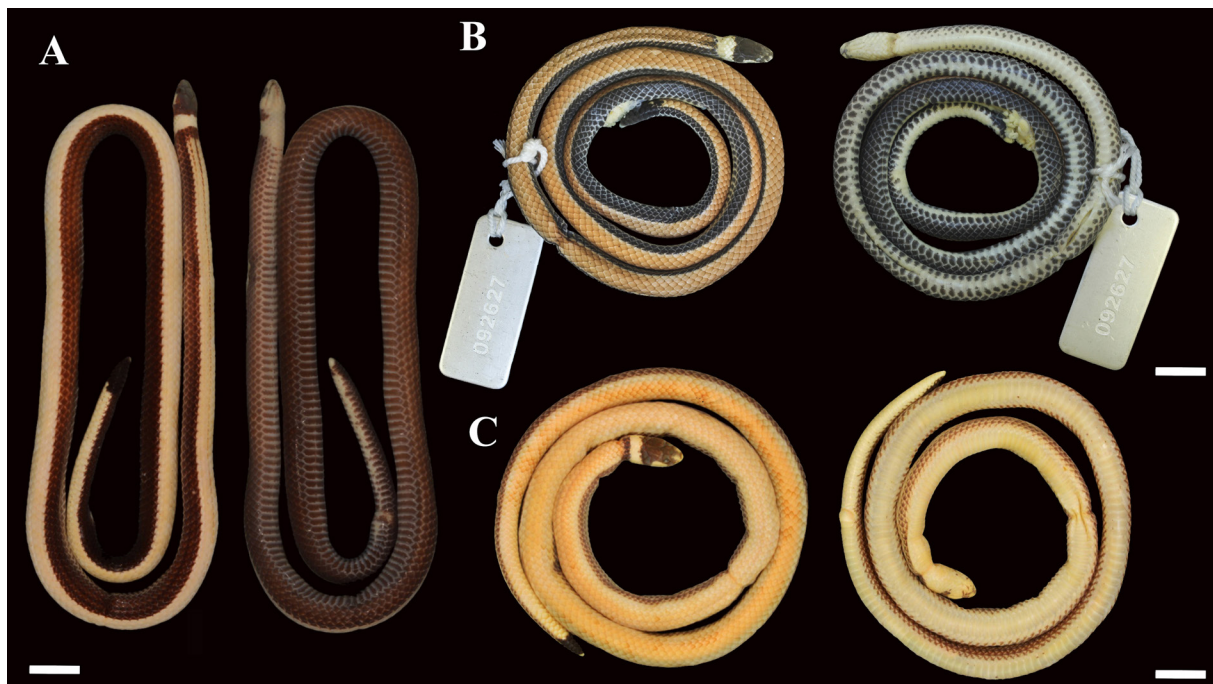Tribe Elapomorphini Jan, 1862
Genus *Apostolepis* Cope, 1862

***Apostolepis albicollaris* Lema, 2002**

Apostolepis albicollaris Lema, 2002: 228. Holotype MCP 8355 (adult male; Fig. 1A), from Distrito Federal, Brasília, Parque Zoológico do Distrito Federal (15.775247º S, 47.922950º W, 1171 m altitude), Distrito Federal, Brazil.

Apostolepis cerradoensis Lema, 2003: 123. Holotype MCP 15219 (adult male; Fig. 1C), from Usina Hidrelétrica de Serra da Mesa, Minaçu (13.510069º S, 48.209950º W, 351 m altitude), Goiás, Brazil. **Syn. nov.**

Heterochresonymy

Apostolepis dimidiata – Lema 1993:35. — Harvey 1999: 408 (in part, misidentification) (figs 1–4, 8).

Fig. 1. Degrees of morphological variation in dorsal and ventral view, of *Apostolepis* Cope, 1862 from the Cerrado. **A**. *Apostolepis albicollaris* Lema, 2002, holotype from Brasília, Distrito Federal, Brazil (MCP 8355). **B**. *Apostolepis albicollaris*, specimen from Ipameri, Goiás, Brazil (IBSP 092627). **C**. *Apostolepis cerradoensis* Lema, 2003, holotype from Minaçu, Goiás, Brazil (MCP 15219). Notice the varying degrees of ventral melanism polymorphism, ranging from uniformly black, to black and cream, and uniformly cream. Photograph credits: Douglas Sebben (A, C), Rafael P. Benetti (B). Scale bars = 10 mm.

Diagnosis

This species presents (1) 15/15/15 dorsal scales; (2) preocular present, contacting nasal; (3) loreal absent (rarely present); (4) temporals absent; (5) supralabials six (rarely four, five, seven), 2nd–3rd in contact with orbit; (6) infralabials six or seven (rarely eight), 1st–4th in contact with anterior chinshields; (7) ventrals 196–230 (196–208 in males; 206–230 in females); (8) subcaudals 24–33 (24–30 in males; 28–33 in females); (9) dorsal pattern uniform orange or red, with two large lateral black stripes (a vestigial vertebral stripe rarely present); (10) ventral pattern uniformly black, bicolor or white; (11) white nuchal collar present, 3–4 wide, black nape collar present (rarely absent), 1.5–3 scales wide; (12) caudal blotch 5–9 scales long on dorsum, incomplete (rarely complete) on venter, terminal scale black and white; (13) supralabial blotch elongated, three to five scales wide; (14) maximum SVL 451 mm, maximum TL 50 mm; (15) hemipenis slightly bilobed, semicapitate, semicalyculate, body covered by moderately sized hooked spines on sulcate side.
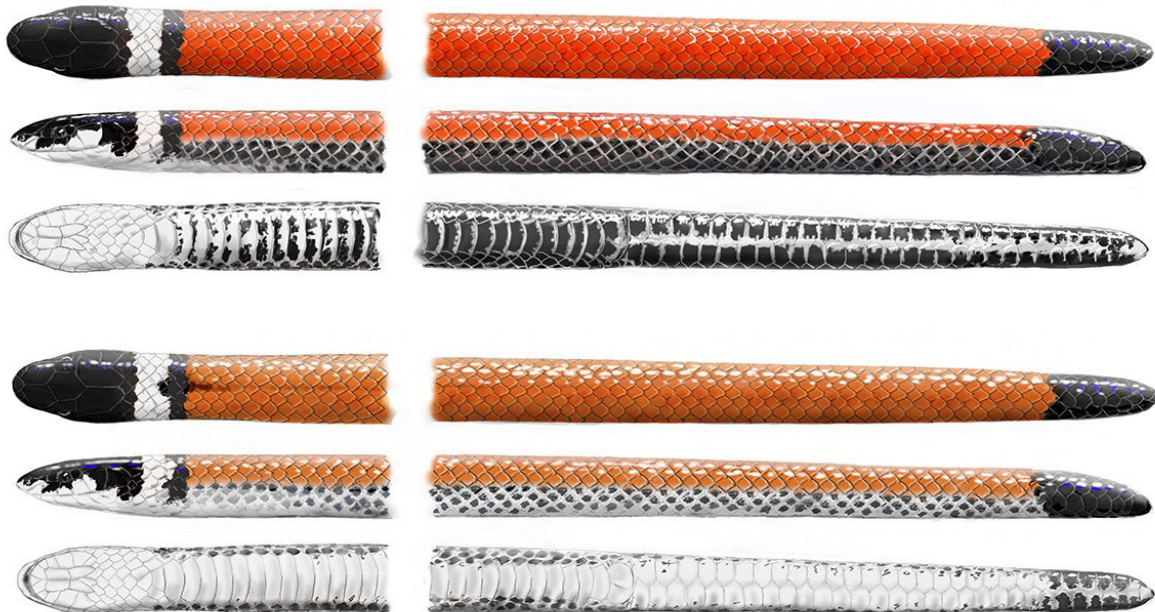
Type material

Holotype
BRAZIL • adult ♀; Distrito Federal, Brasília, Parque Zoológico do Distrito Federal; 15.775247º S, 47.922950º W; alt. 1171 m; MCP 8355 (Fig. 1A).
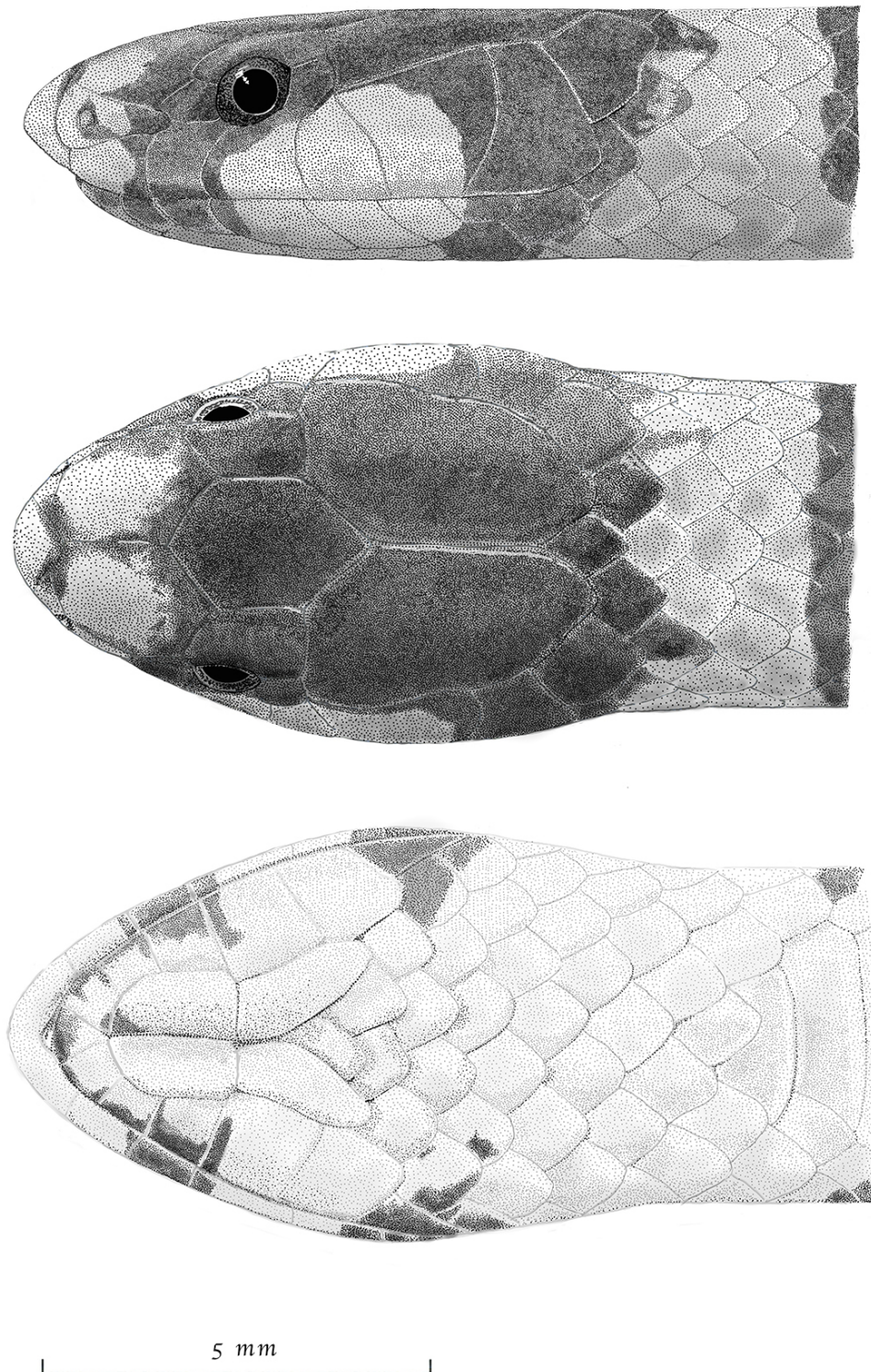
Paratypes (n = 2)
BRAZIL • 1 adult ♀; Goiás, Ipameri; 17.72197º S, 48.1597º W; alt. 64 m; IB1822 • 2 adult ♂♂; Goiás, Minaçu; 13.5331º S, 48.22º W; alt. 351 m; UHESM 18484, 20907.

Description

Head slightly distinct from body, twice as long as wide, triangular in dorsal view, arched in lateral view (Fig. 3); cervical constriction absent; snout conical, tapered in dorsal view, projected in lateral view; nasal

Fig. 2. *Apostolepis albicollaris* Lema, 2002, coloration in life and polymorphism. Holotype of *A. albicollaris* from Brasília, Distrito Federal, Brazil (MCP 8355) (top). Holotype of *Apostolepis cerradoensis* Lema, 2003 from Minaçu, Goiás, Brazil (MCP 15219) (bottom). Drawings: Arthur Tiutenko.

Fig. 3. *Apostolepis albicollaris* Lema, 2002, holotype (MCP 15219) from Minaçu, Goiás, Brazil. Head scalation. Drawings: Arthur Tiutenko.

undivided, longer than wider, in contact with preocular (rarely separated), rostral, first two supralabials and prefrontals; prefrontals paired, longer than wider, in contact with rostral, nasal, supraocular, and frontal; supraocular longer than wider; frontal hexagonal, longer than wider; internasals absent (rarely present); loreal absent (rarely present); preocular present, longer than high; eye small; interorbital distance as long as parietal distance; postocular single, as long as high; temporals absent; occipital present, in contact with parietal and sixth supralabial; supralabials six (rarely four, five, seven), first in contact with nasal and rostral, 2–3 in contact with orbit, 3–4 in contact with postocular, 5–6 in contact with parietal; infralabials six or seven (rarely eight), first pair in contact with symphisal and anterior chinshields, second, third, and fourth pairs in contact with anterior chinshields, third, fourth, fifth, sixth, and seventh pairs in contact with posterior chinshields; dorsal rows 15/15/15; short tail, terminal spine rounded.

Coloration in life

Live specimens have dorsal portion of head black, with snout blotch absent or thin and divided, white or cream colored, covering rostral and prefrontals; white nuchal collar present, 3–4 scales wide; black nape collar present, covering 1.5–3 scales, rarely absent; lateral head portion black, white supralabial blotch elongated, covering three to five scales, infralabials white; ventral portion of head white, with a complete gular black collar; background dorsal coloration red or orange, vertebral stripe vestigial or absent, two lateral black stripes (Fig. 4A–F); ventral coloration uniformly black, bicolor, or white; caudal blotch 5–9 scales wide on dorsum, incomplete (rarely complete) on venter, terminal spine black and white.
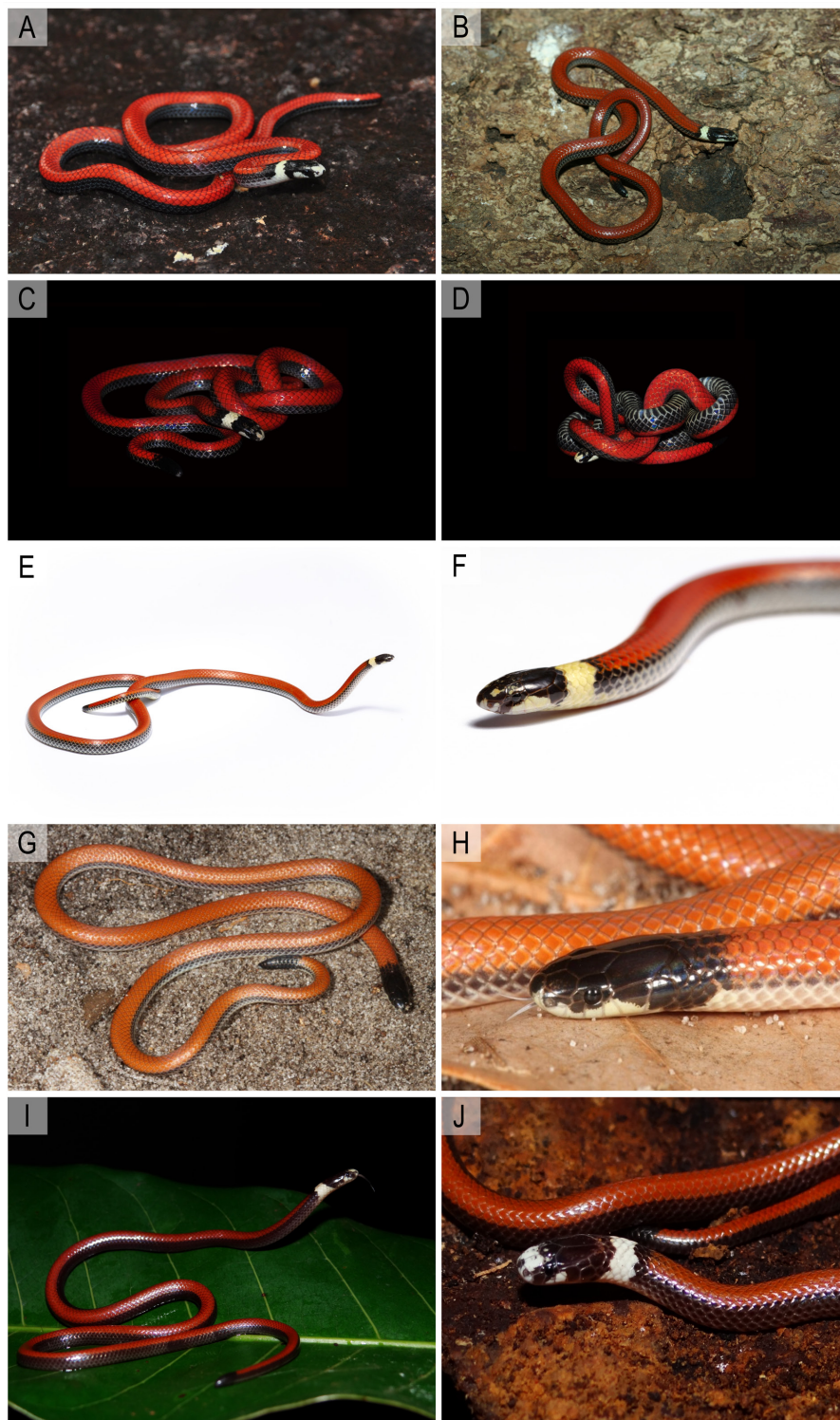
Coloration in preservative

Orange and red colorations turn gray or white in preservative (Fig. 1).

Comparisons

Apostolepis albicollaris might be misidentified as another congener from the Cerrado, *Apostolepis dimidiata* (Fig. 4G–H). Both species share an uniformly red dorsal background coloration, with two lateral black stripes, a white or black venter, and have overlapping scale counts of supralabials, infralabials, and subcaudals. However, *A. albicollaris* can be distinguished from *A. dimidiata* (characters in parentheses) by having nuchal collars (absent), a small-sized semicapitate hemipenis (medium-sized capitate hemipenis), and lower ventral scale counts (220–244 total range, 226–240 in males, 220–244 in females). It should also be noted that *A. dimidiata* is not sympatric with *A. albicollaris* in most of its range, with the former species occurring in the Cerrado of southeastern and central-western Brazil, in the states of São Paulo, Paraná, Minas Gerais, and Mato Grosso do Sul, and in Paraguay, while the latter is restricted to Goiás, Distrito Federal, and Minas Gerais, in central Brazil; both species can be found in sympatry in a small stretch of Cerrado in western Minas Gerais, in the locality of Uberlândia.

Three other similar congeners occur in sympatry with *A. albicollaris*: *Apostolepis assimilis* (Reinhardt, 1861), *Apostolepis flavotorquata* (Duméril, Bibrón & Duméril, 1854), and *Apostolepis sanctaeritae* Werner, 1924. *Apostolepis assimilis* can be diagnosed from *A. albicollaris* based on its dorsal pattern with two black stripes (uniformly red), a divided snout blotch (entire), elongated supralabial blotch, up to five scales wide (smaller, up to three scales wide). *Apostolepis flavotorquata* can be diagnosed from *A. albicollaris* based on its distinct dorsal pattern (uniformly red or with three black stripes), ventral coloration in life (yellow), and hemipenial morphology (organ long and simple, spinules restricted to proximal area, enlarged spines absent, asulcate surface calyculate) (Lema & Renner 2005). *Apostolepis sanctaeritae* can readily be diagnosed from *A. albicollaris* based on its single nuchal collar (additional white nuchal collar), smaller black nuchal collar, covering 1.5–3 scales (4–7 scales), elongated white supralabial blotch (small, tear-shaped), and a divided, white snout blotch in life (single, orange).

Fig. 4. Similar red species of *Apostolepis* Cope, 1862. **A–F**. *Apostolepis albicollaris* Lema, 2002 in life, adult individuals from Brasília, Distrito Federal, Brazil. **G–H**. *Apostolepis dimidiata* (Jan, 1862) in life, adult individual from Laguna Blanca, San Pedro, Paraguay. **I–J**. *Apostolepis quirogai* Giraudo & Scrocchi, 1998 in life, adult individual from Misiones, Argentina. Photograph credits: Cyro de Sousa Bernardes (A, C–D), Luís Felipe Carvalho de Lima (E–F), Jean-Paul Brouard (G–H), Amado Martínez (I–J), and Gabriel Horta (B).

An extralimital species, *Apostolepis quirogai* Giraudo & Scrocchi, 1998, bears striking similarity to *A. albicollaris* (Fig. 4I–J). Both species share a uniformly red dorsal background coloration, with two lateral black stripes, wide white and black nuchal collars, and black ventral coloration. However, *A. albicollaris* can be distinguished from this species based on its lower ventral scale counts (269 in the single male, 276 in the single female), a divided snout blotch (entire), and a larger, elongated, supralabial blotch (smaller, covering up to three scales). Furthermore, *A. quirogai* occurs in Misiones, in northwestern Argentina, and northern Rio Grande do Sul, southern Brazil, in Alto Paraná Atlantic Rainforests, a very distinct environment from the Cerrado of Central Brazil in which *A. albicollaris* occurs.

From *Apostolepis multicincta* Harvey, 1999 and *A. dorbignyi* (Schlegel, 1837), two extralimital species from the Argentine and Bolivian Chaco open areas, *A. albicollaris* can be distinguished based on its dorsal pattern with two lateral black stripes (uniformly red coloration in life), divided snout blotch (entire), and bicolored tail tip (uniformly white).

Furthermore, *A. albicollaris* can be distinguished from *A. adhara* França, Barbo, Silva-Jr, Silva & Zaher, 2018, *A. ambiniger* (Peters, 1869), *A. arenaria* Rodrigues, 1993, *A. borelli* Peracc, 1904, *A. breviceps* Harvey, Gonzales & Scrocchi, 2001, *A. christineae* Lema, 2002, *A. gaboi* Rodrigues, 1993, *A. goiasensis* Prado, 1942, *A. intermedia* Koslowsky, 1898, *A. kikoi* Santos, Entiauspe-Neto, Araújo, Souza, Lema, Strüssmann & Albuquerque, 2018, *A. lineata* Cope, 1887, *A. longicaudata* Gomes, 1921, *A. nelsonjorgei* Lema & Renner, 2004, *A. niceforoi* Amaral, 1935, *A. nigrolineata* (Peters, 1869), *A. nigroterminata* Boulenger, 1896, *A. phillipsi* Harvey, 1999, *A. quirogai* Giraudo & Scrocchi, 1998, *A. rondoni* Amaral, 1925, *A. serrana* Lema & Renner, 2006, *A. striata* Lema, 2004, *A. tenuis* Ruthven, 1927, *A. thalesdelemai* Borges-Nojosa, Lima, Bezerra & James, 2017, *A. underwoodi* Lema & Campbell, 2017, and *A. vittata* (Cope, 1887) based on a combination of its uniformly red dorsal pattern with two lateral black stripes (a different combination of none, three, five, seven, or eleven dorsal stripes, over red, yellow, brown, black or gray background coloration) with the presence of white and black nuchal collars (nuchal collars absent in *A. ambiniger*, *A. breviceps*, *A. christineae*, *A. dimidiata*, *A. goiasensis*, *A. intermedia*, *A. lineata*, *A. longicaudata*, *A. niceforoi*, *A. serrana*, *A. striata*, *A. vittata*, variable for *A. nigrolineata* and *A. thalesdelemai*).

Hemipenis

Hemipenis slightly bilobed, semicapitate, semicalyculate (Fig. 5). Lobes slightly differentiated, present on distal portion of an incomplete capitular ring; lobes rounded, present on distal portion next to incomplete capitulum; lobes and incomplete capitulum covered by papillate calyces on sulcate and lateral sides; incomplete capitulum inconspicuous on both asulcate and sulcate sides, slightly smaller than hemipenial body, and positioned above bifurcation of sulcus spermaticus. Bifurcation of sulcus spermaticus in middle of organ. Capitular groove slightly distinct on sulcate side. Sulcus spermaticus branching centrolineally, with wide invagination on apex and incomplete capitulum; margins of sulcus spermaticus thin and inconspicuous, bordered by expanded lips. Hemipenial body moderately long for *Apostolepis*, subcylindrical; on sulcate surface, hemipenial body covered by small to moderate-sized hooked spines; on asulcate surface, hemipenial body with large basal naked pocket, extended to medial and apical regions, covered by enlarged spines, with inconspicuous lamellae on its asulcate side apex; 1–5 rows of enlarged spines present on lateral portion of sulcate side and medial and apical region of asulcate side.

Sexual dimorphism and variation

Females of *Apostolepis albicollaris* have higher ventrals ($t_{13,9}$ = 44.98, $P < 0.0009$, $n = 22$), and lower subcaudals ($t_{13,9}$ = -34.18, $P < 0.005$, $n = 22$) than their male counterparts (Fig. 6). These results are in agreement with the inferences on sexual dimorphism for *A. albicollaris* encountered by Nogueira

et al. (2012), differing only in detecting sexual dimorphism in subcaudal counts, to which these authors mention a tendency for males to have higher subcaudal counts, but failed to detect statistical differences among sexes. No differences of SVL and TL were encountered, although this might also be attributed to a relatively small sample size between groups. In males, the TL is 9–11% (10 ± 0, $n = 13$) of total length, and SVL is 88–89% (88 ± 0, $n = 13$) of total length, while in females, the TL is 7–9% (8 ± 0, $n = 9$) of total length, and SVL is 90–91% (90 ± 0, $n = 9$) of total length. Males have 197–215 ventrals (204 ± 5.6, $n = 10$), and 29–32 subcaudals (31 ± 1.4, $n = 10$), while females have 206–230 ventrals (216 ± 9.4, $n = 7$), and 24–30 subcaudals (28 ± 2.2, $n = 7$); these values appear to be close to the ones reported for *A. ambiniger* (Entiauspe-Neto *et al.* 2021b).

Geographic distribution and natural history

Known from the states of Goiás, Distrito Federal, and Minas Gerais, central Brazil, in the Cerrado biome (Fig. 7A). The locality reported by Nogueira *et al.* (2019) in Uruaçu, at Poções municipality, Bahia state, is considered here as erroneous. The specimen on which this record is based (IBSP 26712) is reanalyzed herein, and redetermined as being from Cana Brava, on the outskirts of Minaçu municipality, Goiás. *Apostolepis albicollaris* occurs in open areas, with dense shrub vegetation. Nogueira *et al.* (2012) report predation on legless lizards, twilight activity, and reproduction data.

Conservation status

It is known from 37 records representing 17 localities (unique georeferenced coordinates) (Fig. 7A). Its extent of occurrence was calculated to be 62 434 517 km² and its area of occupancy was calculated to be 64 000 km² (B2). The species occurs in less than 10 locations (a). It is under strong pressure by the continued decline in habitat quality by extensive and ongoing habitat loss and fragmentation (b(iii)) due to expansion of agriculture, pasturing, mining, and fire frequency (Fig. 7BC). Additionally, only a small
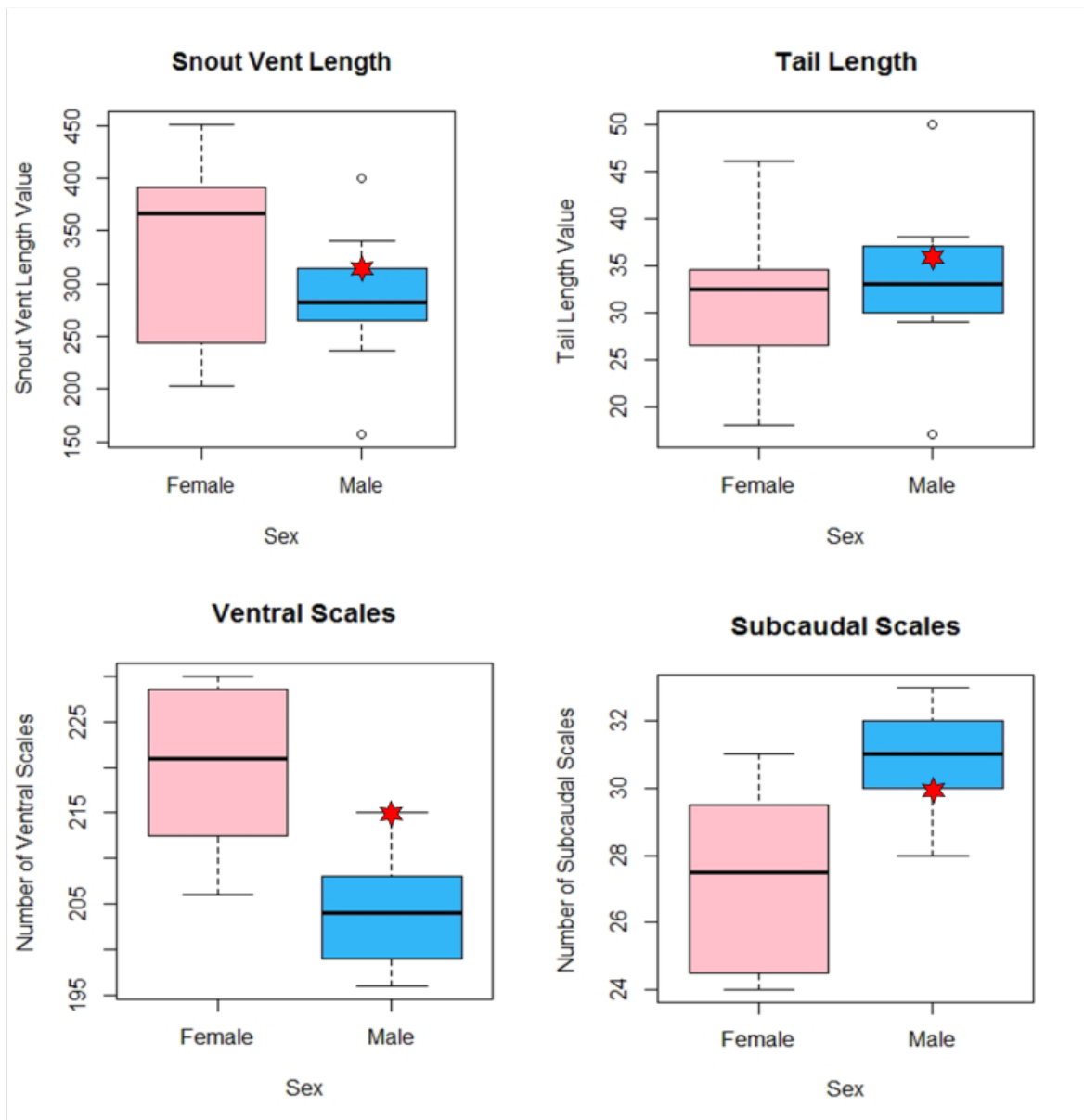

Fig. 5. *Apostolepis albicollaris* Lema, 2002, hemipenis. Sulcate and asulcate sides. Drawings: Arthur Tiutenko.

part of the distribution of the species is located in just one Protected Area (Parque Nacional de Brasília, Fig. 7D). We suggest the species is under threat and qualifies to be listed as Vulnerable (VU ab(iii)).
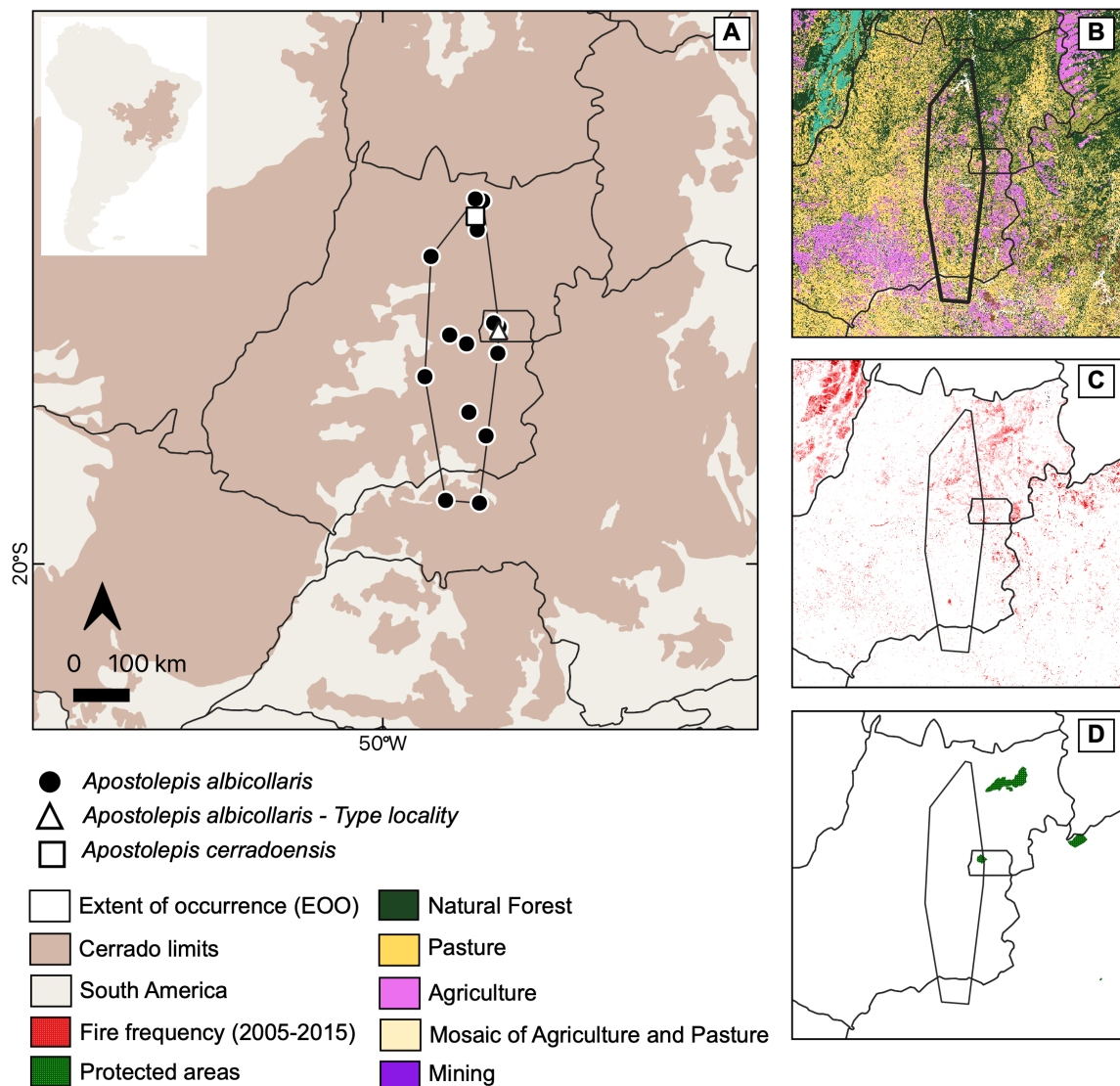
Molecular analyses and systematics

Interspecific uncorrected *p*-distances range from 1 to 7% for *12S* (Table 2) and 0 to 1% for *CMOS* (Table 3). *Apostolepis albicollaris* has a remarkably small genetic difference regarding its putative sister-species, *Apostolepis dimidiata*, having *p*-distances of 1% for *12S* and 0% for *CMOS*. Further studies with larger samples and more molecular markers are needed in order to evaluate the presence or absence of gene flux and monophyletic reciprocity among species. Notably, the small distances recovered for the *CMOS* gene

Fig. 6. *Apostolepis albicollaris* Lema, 2002, sexual dimorphism in morphometric (SVL, TL) and meristic (ventrals, subcaudals) characters. Outliers are indicated as circles, *A. cerradoensis* Lema, 2003 holotype indicated as red star.

indicate that this single-copy, intronless, slow evolving nuclear marker may contain little phylogenetic information for this group, although proven useful for higher level relationships in squamates (Saint *et al.* 1998). Patristic distances among *A. albicollaris* and *A. dimidiata* were recovered as 0.055, and for other species of *Apostolepis* ranged from 0.053 to 0.090 (for *A. flavotorquata* and *A. sanctaeritae*, respectively). The mean interspecific patristic distance for *Apostolepis* is recovered as 0.061, and for the other Elapomorphini genus, *Phalotris,* as 0.116. The results can be seen in Supplementary Table 4.

The phylogenetic trees inferred under maximum likelihood and Bayesian inference recovered as monophyletic the sampled Elapomorphini terminals (*Apostolepis*, *Elapomorphus*, *Phalotris*), with a

Fig. 7. Geographic distribution of *Apostolepis albicollaris* Lema, 2002 in the Cerrado of Central Brazil. **A**. Total range, with minimum convex polygon representing extent of occurrence. **B**. Natural habitat remnants and land use and land cover changes (collection 4, MapBiomas 2021) within the range of *A. albicollaris*. **C**. Fire frequency between 2005 and 2015 (collection 1, MapBiomas 2021) within the range of *A. albicollaris*. **D**. Protected areas (ICMBio 2021) within the range of *A. albicollaris*.

Table 2. Pairwise genetic distances for the *12S* gene among sequences of *Apostolepis* Cope, 1862 analyzed.

	1)	2)	3)	4)	5)	6)
1) *A. albicollaris*						
2) *A. rondoni*	0.04					
3) *A. flavotorquata*	0.06	0.06				
4) *A. dimidiata*	0.01	0.04	0.06			
5) *A. assimilis*	0.06	0.04	0.06	0.06		
6) *A. cearensis*	0.05	0.03	0.05	0.05	0.03	
7) *A. sanctaeritae*	0.07	0.04	0.06	0.07	0.03	0.03

Table 3. Pairwise genetic distances for the *CMOS* gene among sequences of *Apostolepis* Cope, 1862 analyzed.

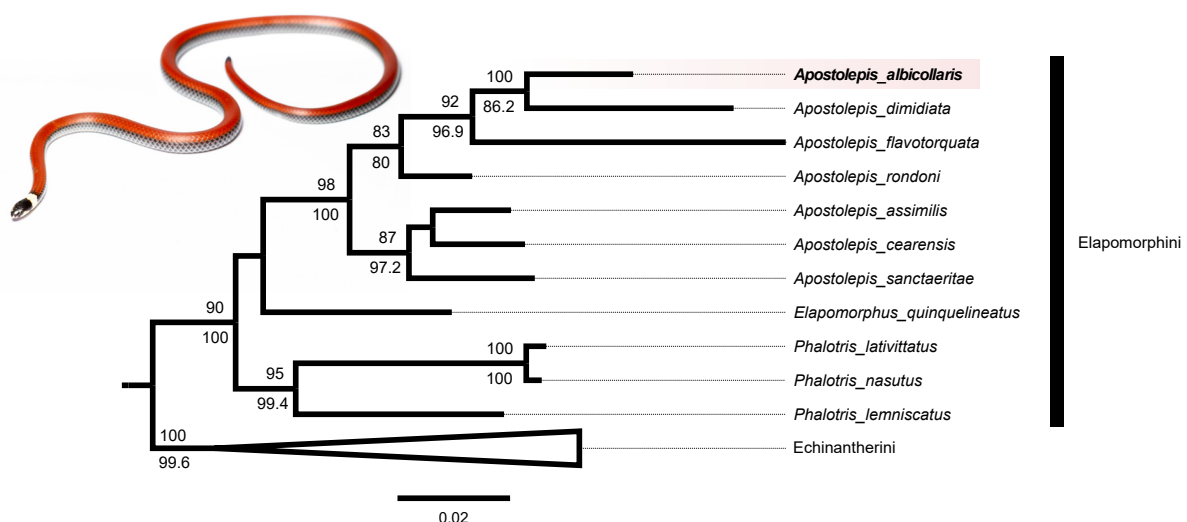|	1)	2)	3)	4)	5)	6)
1) *A. albicollaris*						
2) *A. rondoni*	0.01					
3) *A. flavotorquata*	0.01	0				
4) *A. dimidiata*	0	0	0			
5) *A. assimilis*	0.01	0	0	0		
6) *A. cearensis*	0.01	0	0	0	0	
7) *A. sanctaeritae*	0.01	0.01	0.01	0	0	0

final ML optimized likelihood of –lnL = –12757.360116. All Elapomorphini terminals are recovered as a sister group to Echinantherini genera. Both trees largely agree with each other regarding internal nodes within our clade of interest (Elapomorphini), and are depicted with a maximum likelihood topology and node values for both bootstrap (maximum likelihood) and consensus support (Bayesian inference) (Fig. 8). A clade composed of *A. albicollaris* and *A. dimidiata* is recovered as strongly supported, sister to *A. flavotorquata*, another red congener from the Cerrado. The *Apostolepis assimilis* species group (sensu Ferrarezzi 1993; Ferrarezzi *et al.* 2005), composed of *A. assimilis*, *A. cearensis*, and *A. sanctaeritae*, is also recovered as monophyletic. Regarding the intrageneric and intergeneric relationships of *Apostolepis* terminals, our topology agrees with the one presented by Zaher *et al.* (2019).
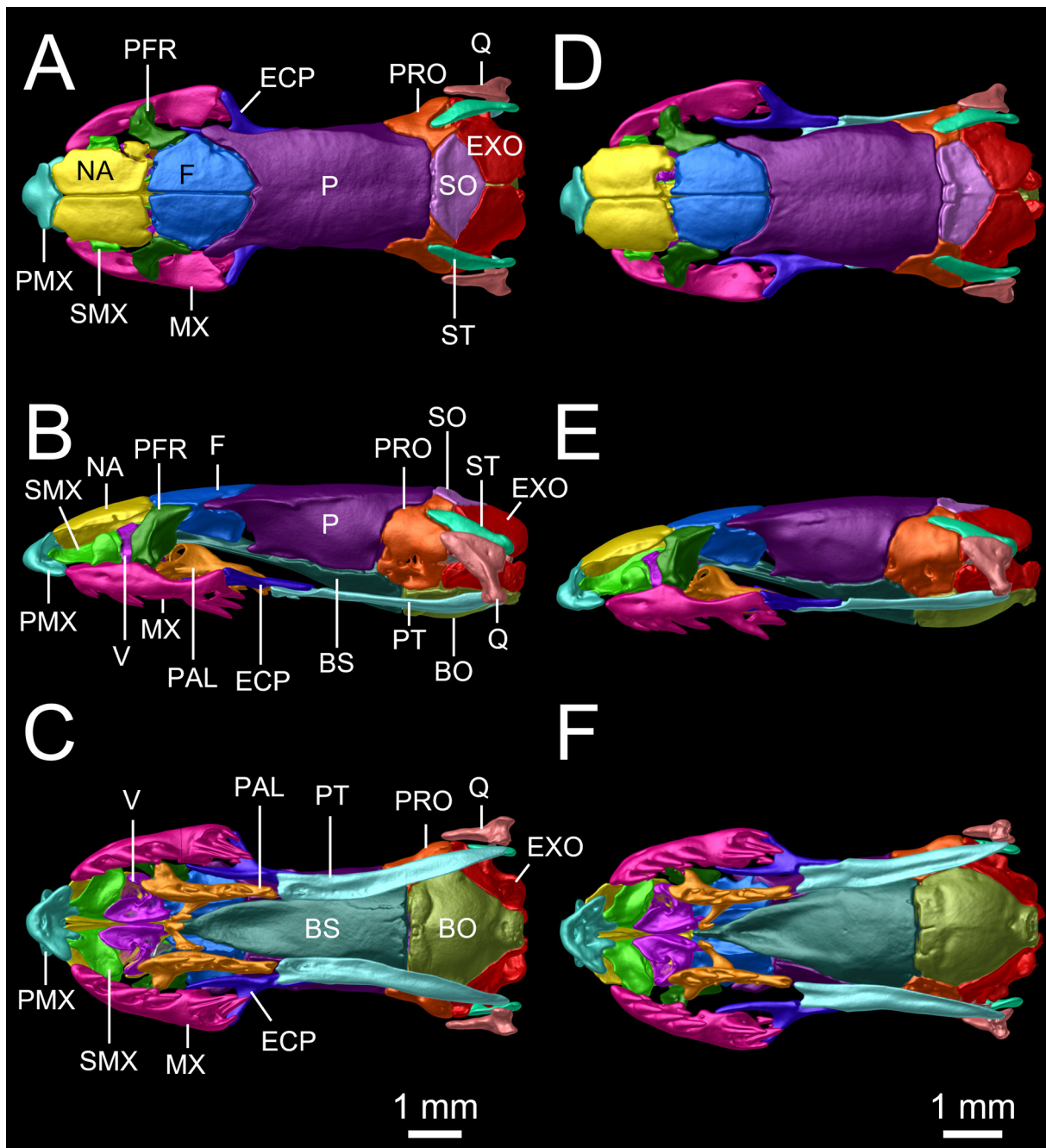
Snout osteology

Snout complex consists of premaxilla, nasals, septomaxillae, vomers, and prefrontals (Figs 9–10).

Premaxilla single, thick, robust, and edentulous, 1.5 (MCP 15219) to 1.6 (MCP 8355) times as broad as high; posterodorsally oriented ascending process has two broad lateral wings and a triangular dorsal apex, contacting anterior end of nasals; transverse processes are posterolaterally oriented, define widest part of premaxilla and are partly visible (MCP 8355) or not (MCP 15219) in dorsal view, long, approaching but not contacting maxillae; posteriorly oriented vomerine processes are robust thumb-like and almost parallel (MCP 15219) or slightly laterally diverging (MCP 8355), with a blunt tip, dorsally contacting anteroventral part of septomaxilla, distinctly separated from anterior end of vomers; ventral surface of premaxilla pierced by a slit-like foramen in anterior region and may have further perforations or notches (MCP 15219).

Nasals paired, more or less rectangular in dorsal view, 1.8 (MCP 15219) to 2.2 (MCP 8355) times as long as broad, convex, in medial contact along a straight suture, with front edges forming a broad V-shaped anterior region, together framing ascending process of premaxilla; lateral edges slightly curved downwards; posteriorly each nasal shares a loose, slightly oblique suture with corresponding frontal, although right nasal of MCP 15219 has a deep, almost circular indentation posteromedially,

Fig. 8. Consensus topology of *Apostolepis* Cope, 1862 BI and ML phylogenetic relationships, support given in Bootstrap (top, > 80) for maximum likelihood inference and Consensus Support (bottom, > 80) for Bayesian inference. Scale bar = molecular distance. Inset photograph: *Apostolepis albicollaris* Lema, 2002 by Luís Felipe Carvalho de Lima.

Fig. 9. Dorsal (A, D), lateral (B, E), and ventral (C, F) views of the skull based on μCT imagery. **A–C**. *Apostolepis albicollaris* Lema, 2002, holotype (MCP 8355). **D–F**. *A. cerradoensis* Lema, 2003, holotype (MCP 15219). Different skull elements are digitally colored and the mandible is removed for better visualization. Abbreviations: BO = basioccipital; BS = basisphenoid; ECP = ectopterygoid; EXO = exoccipital; F = frontal; MX = maxilla; NA = nasal; P = parietal; PAL = palatine; PFR = prefrontal; PMX = premaxilla; PRO = prootic; PT = pterygoid; Q = quadrate; SMX = septomaxilla; SO = supraoccipital; ST = supratemporal; V = vomer.

161

which means that this nasal is hardly in contact with frontal; posterolaterally a small contact region with prefrontal; posteroventral process of nasal contacts anteroventral process of frontal posteriorly and anterior tip of dorsally oriented process of parasphenoid rostrum ventrally; vertical lamina of nasals laterally contacting medial edge of septomaxillae.

Septomaxillae paired and 1.8 (MCP 15219) to 2 (MCP 8355) times as long as broad, separated from each other by vertical laminae of nasals; each with a broad ascending conchal process, freely extending laterally beyond lateral edge of nasal in dorsal view, but not reaching height of lateral nasal edge; anteromedial process of septomaxilla one-fifth (MCP 8355) to one-sixth (MCP 15219) of total length of septomaxilla, curved and oriented anterolaterally, each extending over half depth of premaxilla and contacting posterior lamina of lateral wing of premaxillary ascending process, not visible in dorsal view; posteromedial process long and thin, accounts for 43% (MCP 8355) to 45% (MCP 15219) of total length of septomaxilla, contacts vertical lamina of nasal medially, rounded posterior tip contacts anteroventral tip of frontal, just lateral to ventral contact region between nasal and frontal; septomaxillary body a complex structure partly made of only thin bone material with a rounded indentation in rear view; anterior region of septomaxillary body medially contacting dorsal surface of premaxillary vomerine process; posterior region of septomaxillary body and ventral surface of posteromedial process of septomaxilla contact anterior and dorsal region of vomer.

Vomers paired, complex structures, about 1.4 times as long as wide, medially in contact, and with anterior and posterior regions diverging; anteriorly and dorsally contacting septomaxilla, laterally contacting anterior region of palatine; body of vomer made of thin bone material and globular, with an anteriorly oriented opening; bifurcate vertical posteromedial laminae diverging dorsally and ventrally, framing but not contacting anterior region of choanal process of palatine.

Prefrontals paired, oriented vertically and slightly oblique, 1.7 (MCP 8355) to 1.9 (MCP 15219) times as high as wide, greatly separated from each other, forming anterior margin of orbit; in lateral view, anterior margin undulated (MCP 15219) or convex (MCP 8355); posterolateral margin slightly concave; anterodorsally a small contact region with posterolateral region of nasal; dorsal edge contacts anterolateral edge of frontal along a slightly oblique suture; ventral edge firmly contacts dorsal surfaces of maxilla and of maxillary process of palatine; in rear view, a large, slightly oval lacrimal foramen visible in ventromedial region.
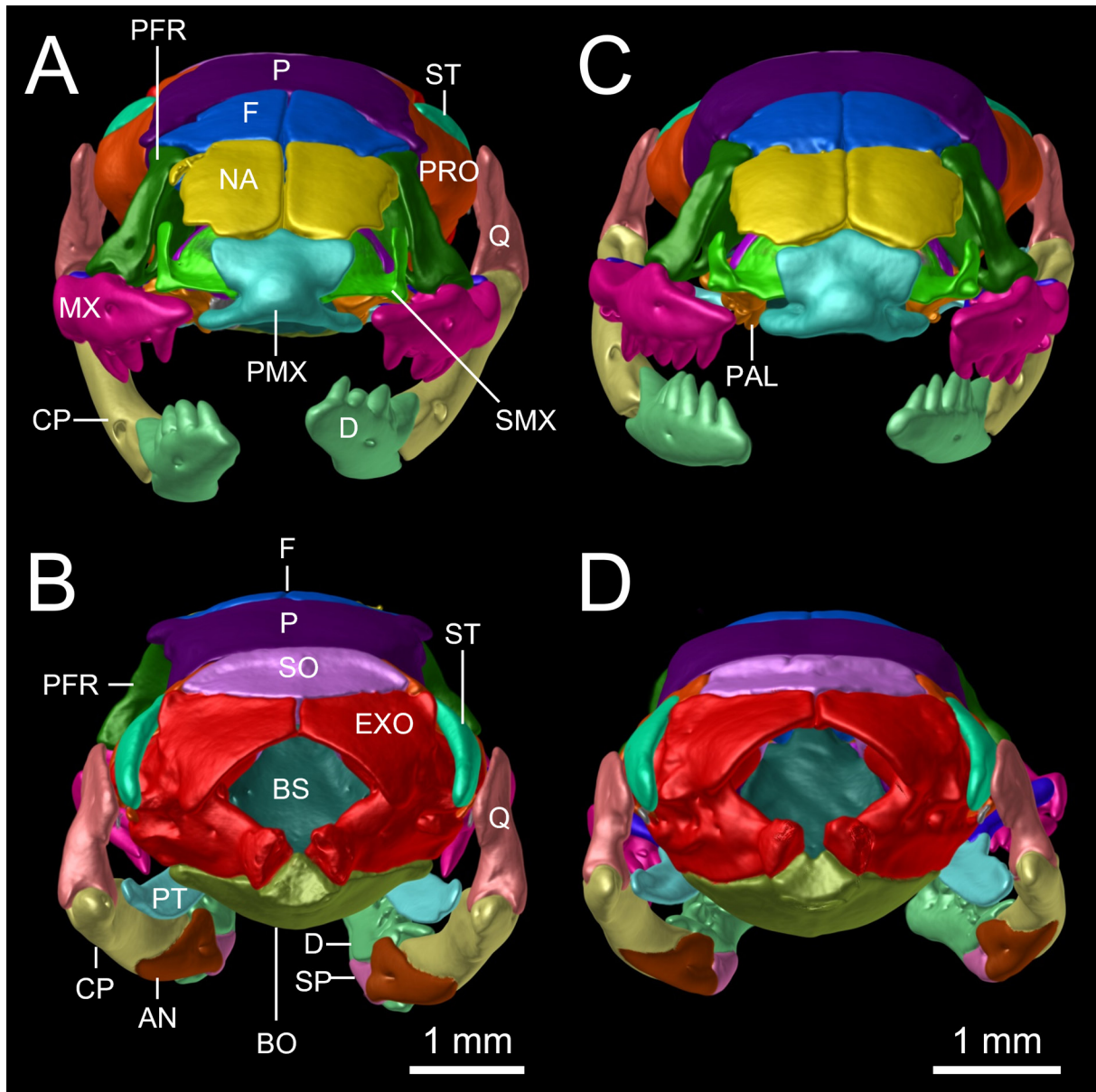
Braincase osteology

Braincase composed of frontals, parietal, supraoccipital, prootics, exoccipitals, parabasisphenoid, and basioccipital (Figs 9–10).

Frontals paired, about semicircular in dorsal view, about 1.8 (MCP 15219) to 2 (MCP 8355) times as long as wide, slightly convex, in medial contact with a straight suture; only a short part of lateral margin of each frontal, at region of greatest width of frontal, participates in formation of dorsal margin of orbit; anterior edge slightly oblique, forming a loose suture with posterior edge of nasal; anterolateral edge forming an oblique suture with prefrontal; posterior edge curved and framed by anterolateral processes of parietal; anteroventrally frontal contacts nasal and directly lateral to this contact zone has a bulge whose anterior surface contacts posterior end of posteromedial process of septomaxilla; laterally each frontal has a ventromedially oriented concave lamina, that contacts its counterpart medially along anterior third of its length; anteromedially, frontal exhibits a vertical lamina fused ventrally with lateral lamina to form a short tubular structure in anterior region of each frontal, with vertical laminae of both frontals in firm medial contact; posterior to tubular structure, lateral lamina of both frontals clearly separated, with their medial margins approximately parallel to each other; on ventral side of contact zone of vertical lamina of frontal a facet into which anterior part of dorsal process of parabasisphenoid penetrates, behind it

dorsal process of parasphenoid protrudes into gap between both lateral laminae and contacts them with its lateral edges.

Parietal single, elongate, 1.4 (MCP 15219) to 1.8 (MCP 8355) times as long as wide, roughly rectangular in dorsal view except for anterolateral processes; dorsal surface slightly convex, except for a slight depression longitudinally along its midline; anterolateral processes moderately long and robust, framing

Fig. 10. Anterior (A, C) and posterior (B, D) views of the skull and lower jaw based on μCT imagery. **A–B**. *Apostolepis albicollaris* Lema, 2002, holotype (MCP 8355). **C–D**. *A. cerradoensis* Lema, 2003, holotype (MCP 15219). Different skull elements are digitally colored to improve visualization. Abbreviations: AN = angular; BO = basioccipital; BS = basisphenoid; CP = compound bone; D = dentary; EXO = exoccipital; F = frontal; MX = maxilla; NA = nasal; P = parietal; PAL = palatine; PFR = prefrontal; PMX = premaxilla; PRO = prootic; PT = pterygoid; Q = quadrate; SMX = septomaxilla; SO = supraoccipital; SP = splenial; ST = supratemporal.

163

posterolateral borders of frontals and forming posterodorsal margins of orbits; anterior border strongly concave curved and posterior border almost straight in transverse direction; anterolateral processes diverge slightly laterally anteriorly; in dorsal view, parietal completely covers pterygoids (MCP 8355) or pterygoids partially visible laterally (MCP 15219); a weakly (MCP 15219) to moderately (MCP 8355) pronounced ridge extends dorsally on both sides of parietal from anterolateral process in posterior direction and almost reaches posterior margin of parietal, and even if both ridges slightly approach each other posteriorly, they remain clearly separated from each other; lateral to dorsal ridges, parietal slopes downwards forming a slightly concave surface in anterior region and a slightly convex surface in posterior region in lateral view; ventrally, parietal meets posterior half of parasphenoid rostrum and most of basisphenoid portion of parabasisphenoid; posterolaterally, parietal contacts anterior and dorsal margin of each prootic and forms anterior border of foramen for maxillary branch of trigeminal nerve at lateral suture with prootic; posterodorsal region of parietal forms an almost straight suture with supraoccipital.

Postorbitals absent.

Supraoccipital single, pentagonal, with straight anterior border and triangular posterior border, about twice as wide as long, slightly concave, and with anterior region slightly elevated; anteriorly it contacts parietal along a straight transverse suture, anterolaterally prootics with an slightly (MCP 15219) to strongly (MCP 8355) oblique suture, and posteriorly exoccipitals with an oblique suture; MCP 15219 has a short elongated notch anterodorsally right and left of midline, respectively, distinctly separated from supratemporals; internally, lateral borders of supraoccipital extend downwards to contribute to dorsomedial walls of otic capsules.

Prootics paired, ovaloid in lateral view, 1.2 (MCP 15219) to 1.45 (MCP 8355) times as high as long; each prootic contacts parietal anteriorly, supraoccipital dorsally, exoccipital posteriorly, parabasisphenoid complex anteroventrally, basioccipital posteroventrally, and anterior part of supratemporal on its dorsal surface; at suture with parietal, prootic forms posterior border of foramen for maxillary branch of trigeminal nerve and at suture with exoccipital it forms anterior margin of fenestra ovalis; slightly posterior and slightly below central part of prootic in lateral view a posterolaterally oriented foramen for mandibular branch of trigeminal nerve; two further foramina on lateral surface of prootic situated in between and ventral to both trigeminal nerve foramina; in dorsal view, prootic bears a depression in posterior region in which rests anterior tip of supratemporal; internally, prootic contributes to formation of anteroventral, anteromedial and anterolateral wall of otic capsule; few small foramina pierce medial laminae of each exoccipital.

Exoccipitals paired, irregularly shaped, and in medial contact along a straight suture; each has a moderately pronounced, dorsolateral ridge; anterodorsally, each exoccipital contacts supraoccipital with a straight, oblique suture, anterolaterally prootic, ventrally basioccipital and dorsolaterally, lateral to dorsal ridge, supratemporal; fenestra ovalis situated at suture between prootic and exoccipital, and exoccipital forms posterior margin of fenestra; posterior to fenestra ovalis halfway to foramen magnum a recess, bearing several foramina; internally, exoccipital contributes to formation of posteroventral, posteromedial and posterolateral wall of otic capsule; exoccipital most posteriorly projecting bone of skull roof and forms dorsal, lateral, and lateroventral border of foramen magnum, with exoccipital components of occipital condyle approaching but remaining slightly separated from each other, posterior process of basioccipital not excluded from participation in foramen magnum.

Parasphenoid and basisphenoid single and fused to form elongate parabasisphenoid, about 1.9 (MCP 15219) to 2.1 (MCP 8355) times as long as wide, and occupying most of skull floor; parabasisphenoid concave in parasphenoid region and convex in basisphenoid region; basisphenoid portion roughly

rounded, parasphenoid rostrum lanceolate with a pointed anterior tip; anterior half of parasphenoid rostrum bears a dorsally oriented process, which protrudes into gap between vertical laminae of frontals, and contacts them with its lateral edges; anterior tip of parasphenoid rostrum does not surpass anterior border of frontals in ventral view; anteriormost part of dorsal process of parasphenoid rostrum contacts ventral surface of posteromedial region of nasals; parasphenoid rostrum distinctly separated from choanal process of palatine, from posterior ending of vomers, and from septomaxillae; dorsolaterally parabasisphenoid contacts frontals and parietal, and prootics posterior to it, and reaches greatest width at sutures between parietal and prootics; foramen located only on right side (both specimens) in posterolateral part of basisphenoid portion, at suture with prootic; in dorsal view (internally), parabasisphenoid pierced by some foramina in lateral region of bone.

Basioccipital single, about hexagonal, almost as wide as long, convex; contacts parabasisphenoid complex anteriorly with straight transverse suture, prootics anterolaterally with oblique sutures, and exoccipitals posterolaterally with oblique sutures; posterodorsally, basioccipital partly overlain by exoccipital components of occipital condyle; posterior end of basioccipital (part of occipital condyle), rectangular-shaped in ventral view and quadrant-shaped in posterior view; widest part of basioccipital at (MCP 15219) or slightly posterior (MCP 8355) to sutures with prootics and exoccipitals; ventral surface of basioccipital slightly elevated in anterior region; small foramen present medially in posterior region, at about where basioccipital part of occipital condyle begins.

Palatomaxillary arch osteology

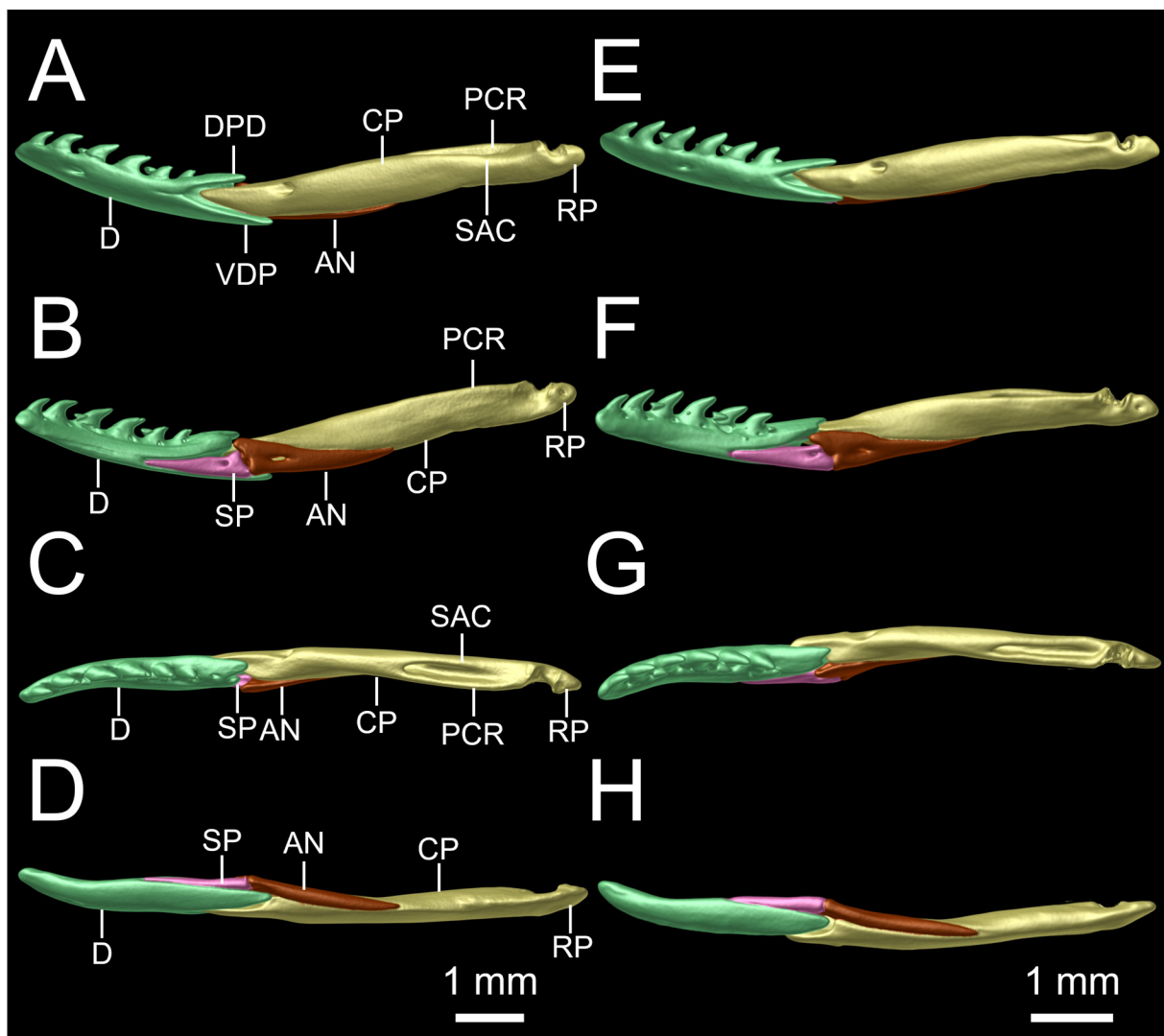Palatomaxillary arch composed of maxillae, ectopterygoids, palatines, and pterygoids (Fig. 11).

Maxillae paired, elongate, account for about one-third of length of skull, about 4.5 (MCP8355) to 4.8 (MCP 15219) times as long as high, each extending from level of (MCP 8355) or shortly behind (MCP 15219) lateral process of premaxilla to posterior region of orbit, forming most of lower margin of orbit laterally; in lateral view, highest point at about mid-length of bone; anteriorly, maxillae slightly arched towards premaxilla; ventral surface of maxilla bears four tooth loci, with curved, and rear-facing anterior teeth approximately similar in size, followed posteriorly, after a small interspace, by a pair of larger and grooved fangs, situated below eye; posterior end of maxilla bears a tooth-like spur at lateral margin of ventral surface; maxilla contacts prefrontal on its dorsal surface at its highest point, anterior regions of lateral and medial processes of ectopterygoid posteriorly, and its short, knob-like palatine process contacts maxillary process of palatine (MCP 8355), or remains slightly separated from it (MCP 15219); a small, knob-like ectopterygoid process visible, but situated slightly anterior to contact zone with anterior tip of medial process of ectopterygoid.

Ectopterygoids paired, wishbone-shaped, deeply forked anteriorly, with a medial process 1.4 (MCP 8355) to 1.9 (MCP 15219) times as long as lateral process; in dorsal view, ectopterygoids either almost entirely visible (MCP 15219) or almost only lateral processes visible and rest of ectopterygoids covered by parietal (MCP 8355); anterior processes directed anterolaterally and frame posterior end of maxilla, forming a maxilo-ectopterygoid fenestra; ventral surface of flattened posterior process has facet, where it firmly contacts dorsal surface of anterolateral portion of pterygoid.

Pterygoids paired, either edentulous (MCP 15219) or with one small tooth in anterior region (MCP 8355), flattened, elongate and slender, 7.5 (MCP 15219) to 8.9 (MCP 8355) times as long as broad, corresponding to slightly less than half length of skull; not in contact with other skull bones except for firm contact with ectopterygoid; in dorsal view, pterygoids only partly (MCP 15219) visible or not visible at all (MCP 8355), completely covered by roofing skull bones; anteromedial tip of pterygoid approaching but not contacting palatine, either thumb-like (MCP 15219) or not pronounced (MCP 8355); in ventral view, lateral border of pterygoid slightly curved posterolaterally; medial borders of pterygoids nearly parallel

to each other in anterior third, gradually diverging and tapering posterolaterally in posterior two-thirds, resulting in greatest distance between both pterygoids at their posterior tips; posterior end of pterygoid approaches ventromedial process of quadrate medially without touching it.

Palatines paired elongate and slender, about 6.2 (MCP 15219) to 6.3 (MCP 8355) times as long as wide, when not considering choanal and maxillary processes, and correspond to 25% (MCP 15219) to 27% (MCP 8355) of length of skull; medial edge slightly curved; ventral surface has three (MCP 8355), four (MCP 15219, left), or five (MCP 15219, right) tooth loci; teeth subequal, curved, and rear-facing; maxillary process of palatine contacts medioventral region of prefrontal on dorsal surface of its maxillary process, and palatine process of maxilla (MCP 8355), or remains slightly separated from it (MCP 15219); anterior portion of palatine, anterior to tooth line almost triangular and contacts ventrolateral

Fig. 11. Lateral (A, E), medial (B, F), dorsal (C, G), and ventral (D, H) views of the lower jaw based on µCT imagery. **A–D**. *Apostolepis albicollaris* Lema, 2002, holotype (MCP 8355). **E–H**. *A. cerradoensis* Lema, 2003, holotype (MCP 15219). Different skull elements are digitally colored to improve visualization. Abbreviations: AN = angular; CP = compound bone; D = dentary; DPD = dorsal process of dentary; PCR = prearticular crest of compound bone; RP = retroarticular process of compound bone; SAC = surangular crest of compound bone; SP = splenial; VDP = ventral process of dentary.

part of vomer dorsally; dorsomedially, a long, thin choanal process rises and curves downwards in a semicircle, approaching but remaining separated from its counterpart medially; short, broad maxillary process situated on lateral surface of palatine at level of first tooth, directed anterolaterally; posterior part of palatine behind tooth line bifurcated, with equally long processes (MCP 15219) or slightly shorter ventrolateral process and slightly longer dorsomedial process (MCP 8355), both tapering towards posterior end.

Suspensorium and mandible osteology

Suspensorium composed of supratemporals and quadrates (Fig. 10). Each mandible composed of dentary, splenial, angular, and compound bone (Fig. 11).

Supratemporals laminar, elongate, more than five times as long as wide, slightly curved, and slightly oblique; in dorsal view, each supratemporal overlaps and firmly contacts more than posterior half of prootic and anterolateral part of exoccipital over well-defined facets; anteriorly approaching, but not reaching to parietal; posterolateral region approaches dorsomedial aspect of quadrate, without touching it; posterior end protrudes posteriorly slightly beyond dorsal region of quadrate, but ends before posterior end of exoccipital.

Quadrates flattened and broad dorsally, tapering dorsoventrally in lateral view, but gradually increasing in width in rear view; oriented obliquely, from anterodorsally to posteroventrally; posterodorsal part approaches posterolateral region of supratemporal medially; medial part has a short process, which corresponds to contact region with columella auris, but columella auris hardly visible; ventral part bifurcated, with medial branch broader than lateral branch and both together spanning glenoid cavity of retroarticular process of mandible; quadrate does not exceed posterior limit of skull roof.

Dentaries elongate and slender, making up about 43% (MCP 15219) to 47% (MCP 8355) of length of mandible, slightly curved anteromedially; dorsal surface bears six tooth loci; teeth subequal, curved and rear-facing; lateral face slightly convex with a mental foramen located at about level of third tooth, in anterior one-third of dentary; at (MCP 8355) or behind (MCP 15219) level of last tooth, dentary branches into a shorter dorsal process, which overlays anterior part of compound bone, and longer lanceolate ventral process; in medial view, gap between dorsal and ventral processes mainly filled by splenial; in ventral view, posteriormost part of ventral process contacts anteroventral part of angular; ventral process runs with its dorsal surface parallel and close along anterior part of medioventral region of compound bone without touching it; in medial view, dorsal process slightly bifurcated in its posteriormost region, distinctly behind last tooth, with a longer dorsolateral branch and a very short ventromedial branch.

Splenials elongate, triangular, tapered anteriorly, about 3.7 (MCP 8355) to 4 (MCP 15219) times as long as high, smallest bone of mandible, making up less than one-fifth of mandibular length; anterior mylohyoid foramen centrally positioned in posterior part of bone anterior to level of its greatest height; posterior edge of splenial firmly contacts anterior region of angular.

Angulars elongate, triangular, tapered posteriorly, almost 4.3 (MCP 8355) to 4.6 (MCP 15219) times as long as high, second smallest bone of mandible, making up a little less than one-third of mandibular length; each angular contacts splenial anteriorly, compound bone laterally and dorsally, posteriormost tip of medial process of dentary, and posteromedial surface of ventral process of dentary; posterior mylohyoid foramen centrally positioned in anterior third of bone.

Compound bones elongate and slender, about 7.3 (MCP 15219) to 8 (MCP 8355) times as long as high, largest bone of mandible, making up more than two-thirds of length of mandible; prearticular crest slightly higher than surangular crest and thus marginally visible in lateral view, the latter not visible in

medial view; in lateral view, compound bone tapers anteriorly, loosely fitting between dorsal and ventral processes of dentary; an anterodorsally oriented foramen present in anterior region on lateral surface of compound bone; retroarticular process moderately long, slightly medially directed, and slightly extends (MCP 8355) or not (MCP 15219) beyond posterior end of exoccipital.

Osteological comparisons

The skull of *A. albicollaris* differs from that of *A. assimilis* (Entiauspe-Neto *et al.* 2021a, characters in parentheses) in having robust thumb-like posterior processes (sharply pointed); weakly to moderately pronounced parietal ridges (well-pronounced); nasal and prefrontal in contact (not in contact); parabasisphenoid and basioccipital bones not fused (fused); anterior end of supratemporal overlaps more than posterior half of prootic and posterior end does not reach posterior end of exoccipital and is not most posteriorly protruding bone of skull roof (anterior end overlaying only posterior part of prootic and posterior end protrudes posteriorly beyond posterior end of exoccipital and is thus most posteriorly protruding bone of skull roof); 0–1 pterygoid teeth (4); parabasisphenoid concave in parasphenoid region (straight); dentary with 6 tooth loci (7–8).

The skull of *A. albicollaris* resembles that of *A. ambiniger* (Entiauspe-Neto *et al.* 2021b, characters in parentheses) but differs from this species in having vomers medially in contact (not contacting each other medially); anterior border of parietal is strongly concave curved (anterior border is almost straight); exoccipital components of occipital condyle approaching but remaining slightly separated from each other, so that posterior process of basioccipital is not excluded from participation in foramen magnum (exoccipital components of occipital condyle are in close contact, excluding posterior process of basioccipital from participation in foramen magnum); prearticular crest is slightly higher than surangular crest of compound bone (prearticular and surangular crests are about similar in height).

It differs from that of *A. cearensis* (Ferrarezzi *et al.* 2005, characters in parentheses) by having 0–1 pterygoid teeth (2); prearticular crest is slightly higher than surangular crest of compound bone (same height as surangular crest); U-shaped fronto-parietal suture in dorsal view without parietal indentation between frontals (W-shaped suture, with an antero-median parietal indentation); dorsal laminae of nasal and frontals in contact (not in contact); dentary with 6 tooth loci (7–8).

The skull of *A. albicollaris* differs from that of *A. sanctaeritae* (Entiauspe-Neto *et al.* 2020a, characters in parentheses) by having dorsal laminae of nasal and frontal in contact (not in contact); nasal and prefrontal in contact (not in contact); 0–1 pterygoid teeth (4–5); weakly to moderately pronounced parietal ridges, both ridges slightly approach each other posteriorly, but remain clearly separated from each other (well-pronounced, both ridges merge in posterior fifth of parietal); dentary with 6 tooth loci (8–9).

Discussion

The number of species of *Apostolepis* is herein reduced to 34. As was the case for *A. cerradoensis*, several species of *Apostolepis* remain known based on a series smaller than five individuals (see Entiauspe-Neto *et al.* 2019). Although Lema (2002) and Nogueira *et al.* (2012) examined relatively large samples of *A. albicollaris* (28 and 14 specimens, respectively), these authors did not account for thorough interspecific comparisons of their evaluated morphological characters, that would reveal it as synonymous with *A. cerradoensis*. It was reported in both studies that *A. albicollaris* might present a white venter, which was considered as a diagnostic character from *A. cerradoensis* (Lema 2003). Other species of *Apostolepis* have also been reported as being highly polymorphic regarding their ventral coloration, such as *A. dimidiata*, which like *A. albicollaris* may also have gradually melanistic ventral coloration (Lema 1993; Entiauspe-Neto *et al.* 2019).

Throughout its range in the Cerrado of Central Brazil, *A. albicollaris* is sympatric or occurs close to at least seven congeners (Table 1). From these, it bears great similarity to *A. dimidiata*, sharing an overlapping dorsal pattern (Fig. 12), coloration, and supralabial, infralabial, and subcaudal counts. These species can be distinguished based on its ventral counts and nuchal collar presence (present in *A. albicollaris*, absent in *A. dimidiata*), and are also not sympatric in most of their ranges, although a small contact zone can be seen in the Cerrado of western Minas Gerais, southeastern Brazil (Nogueira *et al.* 2019). It should also be noted that *A. albicollaris* bears a small-sized semicapitate hemipenis, while *A. dimidiata* bears a medium-sized capitate hemipenis, with enlarged spines in three rows, with spinulate apices; the small sample precludes us from defining these subtle characters as diagnostic or not, although for the time being, we will treat them as such. It is noteworthy that *A. albicollaris*, *A. ambiniger*, *A. dimidiata*, *A. goiasensis*, and *A. kikoi* share similarly small to moderately sized hemipenes, covered by spinules on apical and medial surfaces, with papillate calyces on sulcate and lateral sides, and lamellae on their asulcate sides, which may bear minor interspecific differences, such as the incomplete capitulum on *A. albicollaris*, the well-developed enlarged lateral spines in *A. ambiniger*, *A. goiasensis* and *A. kikoi*, and the conspicuous lamellae on the asulcate side on *A. dimidiata*.

Both *Apostolepis albicollaris* and *A. dimidiata* have been recovered as sister-species in our phylogenetic inferences, and are shown here to have a particularly small degree of molecular difference (*p*-distances of 1% for *12S* and 0% for *CMOS*). Small genetic distances among both species are also supported by the use of patristic distances. We believe that the use of finer and larger molecular markers, such as ultraconserved elements (UCEs) or Restriction site-associated DNA sequencing (RAD-seq), should allow for the evaluation of gene flux, divergence time estimation among lineages, and testing of reciprocal monophyly among these species. Our results are also in contrast with the position of Nogueira *et al.* (2012), who proposed the *Apostolepis dimidiata* species group, containing *A. ambiniger*, *A. albicollaris*, *A. breviceps*, *A. dimidiata*, *A. goiasensis*, *A. intermedia*, *A. lineata*, *A. phillipsi*, *A. vittata*, and *Parapostolepis polylepis* (Amaral, 1922), and claimed that "no putative synapomorphy was found to support a sister-group relationship between these species" (for *A. albicollaris* and *A. dimidiata*). It should also be noted that no evidence was presented to support the aforementioned claim, and the relationships between *A. albicollaris* and *A. dimidiata* were only briefly mentioned in the abstract section. In general terms, the *A. dimidiata* group (sensu Ferrarezzi 1993) is diagnosed by having a rostral scale prominently enlarged (projected), a rounded terminal shield, naris located in the anterior part of nasal, anterior supralabials bent into the oral border, head narrowing towards snout (triangular), light snout blotches confined anteriorly, obscured to indistinct on prefrontal, and the white supralabial blotch elongated continuously throughout labial margin (Nogueira *et al.* 2012). However, these species also have noteworthy differences in other major diagnostic characters, such as the small-sized and rounded hemipenes for *A. intermedia*, and the elongated hemipenes, without prominent lamellae on its asulcate side, added to 17 dorsal rows without reduction for *P. polylepis*. Furthermore, the aforementioned diagnostic characters of the *A. dimidiata* group also integrally apply to other species, such as *A. christineae*, which bears great resemblance and shares several diagnostic characters with *A. vittata* and was seemingly overlooked in the revision proposed by Nogueira *et al.* (2012).

Another species that bears a striking resemblance to *Apostolepis albicollaris* is *A. quirogai*, that also has a red dorsum with two lateral black stripes, a black head and a white nuchal collar (Fig. 13; Giraudo & Scrocchi 1998; Entiauspe-Neto *et al.* 2021b). However, the latter species occurs in Alto Paraná Atlantic Forests of Misiones, in northwestern Argentina, and northern Rio Grande do Sul, southern Brazil, far from the Cerrado of central Brazil (in which *A. albicollaris* occurs), has a wide circular snout blotch, and also bears a considerably higher count of ventral scales (269 in the single male, 276 in the single female) (Giraudo & Scrocchi 1998). Further molecular and morphological evidence is needed for *A. quirogai* in order to test its phylogenetic relationship regarding *A. albicollaris*, and clarify whether both species are close to each other, or if their similarities are rather a byproduct of convergent evolution.

Fig. 12. *Apostolepis dimidiata* (Jan, 1862), putative sister-species of *Apostolepis albicollaris* Lema, 2002, adult specimen from Estação Ecológica Santa Bárbara, São Paulo, Brazil. Photograph credit: Giordano Rossi.

The small sample size of molecular data available for *Apostolepis* precludes us from making general statements on the systematic relationships of the group. Although *Apostolepis* is recovered as monophyletic by this study and other recent phylogenies (e.g., Zaher *et al.* 2019; Moraes *et al.* 2021), only seven terminals have limited gene fragments available (up to four) for comparison, out of the 34 valid species, and key taxa remain unavailable for comparison. For instance, the monotypic genera *Coronelaps* Lema & Hofstadler-Deiques, 2010 and *Parapostolepis* Amaral, 1930 have not yet been tested under a molecular systematic framework, and their relationships with their close counterparts (*Elapomorphus* and *Apostolepis*, respectively) remain hypothesized largely upon morphological characters interpreted as putatively autapomorphic (Lema & Hofstadler-Deiques 2010).

Nevertheless, the available molecular data provides support for the monophyly of the *Apostolepis assimilis* species group in its current sense (sensu Ferrarezzi 1993; Ferrarezzi *et al.* 2005), being composed of three red colored species (*A. assimilis*, *A. cearensis*, *A. sanctaeritae*) that inhabit the South American Dry Diagonal and share a nasal scale separated from preocular, fifth supralabial

Fig. 13. *Apostolepis quirogai* Giraudo & Scrocchi, 1998, adult specimen from Misiones, Argentina, in dorsal and ventral view. Photograph credits: Amado Martínez.

scale only in contact with parietal, temporals 0+1, terminal scale pointed in a sharp edge (although we have encountered specimens of *A. assimilis* with both pointed and rounded terminal scales), large white internasal blotch covering snout and reaching frontal shield, moderate to extremely broad and sharply evident white and black nucho-cervical collars, dorsal pattern uniformly red, white ventral surface (although some specimens may have a red venter), except gular region which is dark to mostly black pigmented, terminal shield black, undifferentiated from tail tip coloration, Duvernoy's gland moderately developed, harderian gland well developed, reaching temporal region, and adductor jaw muscles moderately developed, reaching dorsal surface of braincase (Ferrarezzi 1993; Ferrarezzi *et al.* 2005). However, these characters might not be shared exclusively by these species; *A. dorbignyi* and *A. multicincta* both have a nasal scale separated from preocular, fifth supralabial in contact with parietal, terminal scale pointed, large white internasal blotch, wide white and black nuchal collars, and a uniformly red dorsal pattern, with major differences from the *A. assimilis* group relying on number of infralabials contacting anterior chinshields (1–3 in *A. dorbignyi* and *A. multicincta*), temporal scales (absent in *A. dorbignyi* and *A. multicincta*), and terminal scale coloration (white in *A. dorbignyi* and *A. multicincta*). Both, *A. dorbignyi* and *A. multicincta,* also occur in the South American Dry Diagonal, in the Chaco of Argentina and Bolivia (Harvey 1999; Burgos-Gallardo *et al.* 2017). The aforementioned morphological differences between *A. dorbignyi* and *A. multicincta* on one hand and species of the *A. assimilis* group on the other are subtle, and as most diagnostic characters of coloration used for *Apostolepis*, likely to be prone to individual variation and polymorphism, as more comprehensive series of specimens become available. We argue that taxonomic approaches based strictly on external morphology are likely to overestimate diversity in fossorial and poorly sampled species, and that further studies and data collection, seeking to integrate internal morphology and molecular studies, are needed in order to increase taxonomic stability and the reliability of diagnoses for Elapomorphini species.

Acknowledgements

References

Bachman S., Moat J., Hill A.W., de la Torre J. & Scott B. 2011. Supporting Red List threat assessments with GeoCAT: geospatial conservation assessment tool. *ZooKeys* 150: 117–126. https://doi.org/10.3897/zookeys.150.2109

Bullock R.E. & Tanner W.W. 1966. A comparative osteological study of two species of Colubridae (*Pituophis* and *Thamnophis*). *Brigham Young University Science Bulletin Biological Series* 8: 1–29.

Burgos-Gallardo F., Baldo J.L., Vilte A. & Scrocchi G. 2017. *Apostolepis multicincta* Harvey 1999 (Squamata, Dipsadidae) in Argentina. *Check List* 13: 913–916. https://doi.org/10.15560/13.6.913

Cabral H., Lema T.D. & Renner M.F. 2017. Revalidation of *Apostolepis barrioi* (Serpentes: Dipsadidae). *Phyllomedusa* 16: 243–254. https://doi.org/10.11606/issn.2316-9079.v16i2p243-254

Cundall D. & Irish F. 2008. The snake skull. *In*: Gans C., Gaunt A.S. & Adler K. (eds) *Biology of Reptilia. The Skull of Lepidosauria*: 349–692. Society for the Study of Amphibians and Reptiles Press, USA.

Curcio F.F., Nunes P.M.S., Harvey M.B. & Rodrigues M.T. 2011. Redescription of *Apostolepis longicaudata* (Serpentes: Xenodontinae) with comments on its hemipenial morphology and natural history. *Herpetologica* 67 (3): 318–331. https://doi.org/10.1655/HERPETOLOGICA-D-10-00043.1

Dowling H.G. 1951. A proposed standard system of counting ventrals in snakes. *British Journal of Herpetology* 1: 97–99.

Drummond A., Ashton B., Buxton S., Cheung M., Cooper A., Duran C. & Wilson A. 2010. Geneious pro. Geneious Biomatters Ltd, Auckland.

Edgar R.C. 2004. MUSCLE: multiple sequence alignment with high accuracy and high throughput. *Nucleic Acids Research* 32 (5): 1792–1797. https://doi.org/10.1093/nar/gkh340

Entiauspe-Neto O.M., de Sena A., Tiutenko A. & Loebmann D. 2019. Taxonomic status of *Apostolepis barrioi* Lema, 1978, with comments on the taxonomic instability of *Apostolepis* Cope, 1862 (Serpentes, Dipsadidae). *ZooKeys* 841: 71–78. https://doi.org/10.3897/zookeys.841.33404

Entiauspe-Neto O.M., Koch C., Guedes T.B. & Tiutenko A. 2020a. Revisiting the taxonomic status of *Apostolepis sanctaeritae*, a forgotten Neotropical dipsadid snake. *Salamandra* 56: 329–341.

Entiauspe-Neto O.M., Guedes T.B., Loebmann D. & Lema T. 2020b. Taxonomic status of two simultaneously described *Apostolepis* Cope, 1862 species (Dipsadidae: Elapomorphini) from Caatinga Enclaves moist forests, Brazil. *Journal of Herpetology* 54: 225–234. https://doi.org/10.1670/19-053

Entiauspe-Neto O.M., Rangel G.M.F., Guedes T.B. & Tiutenko A. 2020c. Raising of Lazarus: rediscovery and redescription of *Apostolepis niceforoi* Amaral, 1935 (Serpentes: Dipsadidae: Elapomorphini). *Holotipus* 1: 21–35.

Entiauspe-Neto O.M., Koch C., Gray R.J., Tiutenko A., Loebmann D. & Guedes T.B. 2021a. On the identity of *Apostolepis tertulianobeui* Lema, 2004 and integrative revision of *Apostolepis assimilis* (Reinhardt, 1861) (Serpentes: Dipsadidae). *Zoologischer Anzeiger* 291: 123–138. https://doi.org/10.1016/j.jcz.2021.01.004

Entiauspe-Neto O.M., Koch C., Harvey M.B., Colli G.R. & Guedes T.B. 2021b. Redescription of *Apostolepis ambiniger* (Peters, 1869) (Serpentes: Dipsadidae: Elapomorphini). *Vertebrate Zoology* 71: 231–251. https://doi.org/10.3897/vz.71.e65097

Entiauspe-Neto O.M., Abegg A.D., Koch C., Nuñez L.P., Azevedo W.D.S., Moraes L.J., Tiutenko A., Bialves T.S. & Loebmann D. 2021c. A new species of *Erythrolamprus* (Serpentes: Dipsadidae: Xenodontini) from the savannas of northern South America. *Salamandra* 57 (2): 196–218.

Ferrarezzi H. 1993. *Sistemática Filogenética de Elapomorphus, Phalotris e Apostolepis (Serpentes, Colubridae, Xenodontinae)*. PhD thesis, Universidade de São Paulo, Brazil.

Ferrarezzi H. 1994. Uma sinopse dos gêneros e classificação das serpentes (Squamata): II. Família Colubridae. *In*: Nascimento L.B., Bernardes A.T. & Cotta G.A. (eds) *Herpetologia no Brasil* 1: 81–91. PUCMG, Belo Horizonte.

Ferrarezzi H., Barbo F.E. & Albuquerque C.E. 2005. Phylogenetic relationships of a new species of *Apostolepis* from Brazilian Cerrado, with notes on the *assimilis* group (Serpentes: Colubridae: Xenodontinae: Elapomorphini). *Papéis Avulsos de Zoologia* 45: 215–229. https://doi.org/10.1590/S0031-10492005001600001

Giraudo A.R. & Scrocchi G.J. 1998. A new species of *Apostolepis* (Serpentes: Colubridae) and comments on the genus in Argentina. *Herpetologica* 54 (4): 470–476.

Guedes T.B., Nogueira C. & Marques O.A.V. 2014. Diversity, natural history, and geographic distribution of snakes in the Caatinga, Northeastern Brazil. *Zootaxa* 3863 (1): 1–93. https://doi.org/10.11646/zootaxa.3863.1.1

Harvey M.B. 1999. Revision of Bolivian *Apostolepis* (Squamata: Colubridae). *Copeia* 1999: 388–409. https://doi.org/10.2307/1447485

Hasegawa M., Kishino H. & Yano T.A. 1985. Dating of the human-ape splitting by a molecular clock of mitochondrial DNA. *Journal of Molecular Evolution* 22 (2): 160–174. https://doi.org/10.1007/BF02101694

Huelsenbeck J.P. & Ronquist F. 2001. MrBayes: Bayesian inference of phylogenetic trees. *Bioinformatics* 17 (8): 754–755. https://doi.org/10.1093/bioinformatics/17.8.754

ICMBio 2021. Mapa temático e Dados geoestatísticos das Unidades de Conservação Federais. Available from https://icmbio.gov.br [accessed 4 Nov. 2021].

Lema T.D. 1993. Polimorfismo em *Apostolepis dimidiata* (Jan, 1862) com a invalidação de *Apostolepis villaricae* Lema, 1978 e *Apostolepis barrioi* Lema, 1978 (Serpentes: Colubridae: Xenodontinae: Elapomorphini). *Acta Biologica Leopoldensia* 15: 35–52.

Lema T.D. 2002. Nova espécie de *Apostolepis* Cope do grupo *dimidiata* do Cerrado do Brasil (Serpentes: Elapomorphinae). *Comunicações do Museu de Ciências e Tecnologia da PUCRS, Série Zoologia* 15 (2): 227–238.

Lema T.D. 2003. Descrição de nova espécie de *Apostolepis* Cope do cerrado do Brasil, pertencente ao grupo *dimidiata* (Serpentes, Elapomorphinae). *Acta Biologica Leopoldensia* 25 (1): 123–131.

Lema T.D. 2004a. Nova espécie de *Apostolepis* Cope do estado de Rondônia, Brasil (Serpentes, Elapomorphinae). *Comunicações do Museu de Ciências e Tecnologia da PUCRS, Série Zoologia* 17 (2): 81–89.

Lema, T.D. 2004b. Description of a new species of *Apostolepis* Cope, 1861 (Serpentes, Elapomorphinae) from Brazilian Cerrado. *Acta Biologica Leopoldensia* 26 (1): 155–160.

Lema T.D. & Hofstadler-Deiques C. 2010. Description of a new genus for allocation of *Elapomorphus lepidus* and the status of *Elapomorphus wuchereri* (Serpentes: Dipsadidae: Xenodontinae: Elapomorphini). *Neotropical Biology and Conservation* 5 (2): 113–119. https://doi.org/10.4013/4756

Lema T.D. & Renner M.F. 2005. Contribuição ao conhecimento taxonômico de *Apostolepis flavotorquata* (Serpentes, Elapomorphinae). *Biociências* 13 (2): 163–175.

Lema T.D. & Renner M.F. 2011. A new species of *Apostolepis* (Serpentes, Colubridae, Elapomorphini), belonging to *assimilis* group, found in Brazilian Cerrado. *Ciência em Movimento* 13 (27): 71–76.

MapBiomas 2021. Collections 1 and 4 of the Annual Series of Brazilian Land Use and Land Cover. Available from https://mapbiomas.org [accessed 4 Nov. 2021].

Montingelli G.G., Barbo F.E., Pereira Filho G.A., Santana G.G, França F.G.R., Grazziotin F.G. & Zaher H. 2020. A second new species for the rare dipsadid genus *Caaeteboia* Zaher et al., 2009 (Serpentes: Dipsadidae) from the Atlantic Forest of northeastern Brazil. *Cuadernos de Herpetología* 34: 219–230.

Moraes L.J., Entiauspe-Neto O.M., de Fraga R., Fernandes I.Y. & Werneck F.P. 2021. Systematics of the rare Amazonian genus *Eutrachelophis* (Serpentes: Dipsadidae), with an emended diagnosis for *Eutrachelophis papilio*. *Zoologischer Anzeiger* 295: 191–204. https://doi.org/10.1016/j.jcz.2021.10.003

Nogueira C.C., Barbo F.E. & Ferrarezzi H. 2012. Redescription of *Apostolepis albicollaris* Lema, 2002, with a key for the species groups of the genus *Apostolepis* (Serpentes: Dipsadidae: Elapomorphini). *South American Journal of Herpetology* 7 (3): 213–225. https://doi.org/10.2994/057.007.0303

Nogueira C.C., Argôlo A.J.S., Arzamendia V., Azevedo J.A., Barbo F.E., Bérnils R.S., Bolochio B.E., Borges-Martins M., Brasil-Godinho M., Braz H., Buononato M.A., Cisneros-Heredia D.F., Colli G.R., Costa H.C., Franco F.L., Giraudo A., Gonzales R.C., Guedes T., Hoogmoed M.S., Marques O.A.V., Montingelli G.G., Passos P., Prudente A.L.C., Rivas G.A., Sanchez P.M., Serrano F.C., Silva-Jr N.J., Strüssmann C., Vieira-Alencar J.P.S., Zaher H., Sawaya R.J. & Martins M. 2019. Atlas of Brazilian snakes: verified point-locality maps to mitigate the Wallacean shortfall in a megadiverse snake fauna. *South American Journal of Herpetology* 14 (Suppl. 1): 1–274. https://doi.org/10.2994/SAJH-D-19-00120.1

Paradis E. & Schliep K. 2019. ape 5.0: an environment for modern phylogenetics and evolutionary analyses in R. *Bioinformatics* 35 (3): 526–528. https://doi.org/10.1093/bioinformatics/bty633

Peters J.A. 1964. Supplemental notes on snakes of the subfamily Dipsadinae (Reptilia: Colubridae). *Studies on Neotropical Fauna and Environment* 4 (1): 45–50. https://doi.org/10.1080/01650526409360376

QGIS Development Team 2021. QGIS Geographic Information System. Version 3.16.3. Available from http://www.qgis.org [accessed 1 Aug. 2021].

R Core Team 2015. Team R: a language and environment for statistical computing, Release 3.2. Available from http://cran.r-project.org [accessed 1 Aug. 2021].

Rodrigues M.T. 1992. Herpetofauna das dunas interiores do Rio São Francisco: Bahia: Brasil. V. Duas novas espécies de *Apostolepis* (Ophidia, Colubridae). *Memórias do Instituto Butantan* 54 (2): 53–59.

Sabaj M.H. 2019. *Standard Symbolic Codes for Institutional Resource Collections in Herpetology and Ichthyology: An Online Reference.* Version 6.5. American Society of Ichthyologists and Herpetologists, Lawrence, KS. Available from http://www.asih.org [accessed 10 Sep. 2021].

Saint K.M., Austin C.C., Donnellan S.C. & Hutchinson M.N. 1998. C-*mos*, a nuclear marker useful for squamate phylogenetic analysis. *Molecular Phylogenetics and Evolution* 10 (2): 259–263. https://doi.org/10.1006/mpev.1998.0515

Savitzky A.H. 1979. *The Origin of the New World Proteroglyphous Snakes and its Bearing on the Study of Venom Delivery Systems in Snakes*. PhD thesis, University of Kansas, Lawrence, KS.

Souza Jr. C.M., Shimbo J.Z., Rosa M.R., Parente L.L., Alencar A.A., Rudorff B.F.T., Hasenack H., Matsumoto M., Ferreira L.G., Souza-Filho P.W.M., Oliveira S.W., Rocha W.F., Fonseca A.V., Marques C.B., Diniz C.G., Costa D., Monteiro D., Rosa E.R., Vélez-Martin E., Weber E.J., Lenti F.E.B., Paternost F.F., Pareyn F.G.C., Siqueira J.V., Viera J.L., Neto L.C.F., Saraiva M.M., Sales M.H., Salgado M.P.G., Vasconcelos R., Galano S., Mesquita V.V. & Azevedo T. 2020. Reconstructing three decades of land use and land cover changes in Brazilian biomes with Landsat Archive and Earth Engine. *Remote Sensing* 12 (7): e2735. https://doi.org/10.3390/rs12172735

Stamatakis A. 2014. RAxML version 8: a tool for phylogenetic analysis and post-analysis of large phylogenies. *Bioinformatics* 30 (9): 1312–1313. https://doi.org/10.1093/bioinformatics/btu033

Tamura K., Peterson D., Peterson N., Stecher G., Nei M. & Kumar S. 2011. MEGA5: Molecular Evolutionary Genetics Analysis using maximum likelihood, evolutionary distance, and maximum parsimony methods. *Molecular Biology and Evolution* 28 (10): 2731–2739. https://doi.org/10.1093/molbev/msr121

Tavaré S. 1986. Some probabilistic and statistical problems in the analysis of DNA sequences. *Lectures on Mathematics in the Life Sciences* 17 (2): 57–86.

Zaher H. 1994. *Phylogénie des Pseudoboini et Évolution des Xenodontinae Sud-américains (Serpentes, Colubridae)*. PhD thesis, Muséum national d'histoire naturelle, Paris.

Zaher H. 1999. Hemipenial morphology of the South American xenodontine snakes, with a proposal for a monophyletic Xenodontinae and a reappraisal of colubroid hemipenes. *Bulletin of the American Museum of Natural History* 240: 1–168. Available from https://www.biodiversitylibrary.org/bibliography/90073 [accessed 6 Apr. 2022].

Zaher H., Grazziotin F.G., Cadle J.E., Murphy R.W., Moura-Leite J.C.D. & Bonatto S.L. 2009. Molecular phylogeny of advanced snakes (Serpentes, Caenophidia) with an emphasis on South American Xenodontines: a revised classification and descriptions of new taxa. *Papéis Avulsos de Zoologia* 49: 115–153. https://doi.org/10.1590/S0031-10492009001100001

Zaher H., Murphy R.W., Arredondo J.C., Graboski R., Machado-Filho P.R., Mahlow K., Montingelli G.G., Quadros A.B., Orlov N.L., Wilkinson M., Zhang Y.-P. & Grazziotin F.G. 2019. Large-scale molecular phylogeny, morphology, divergence-time estimation, and the fossil record of advanced caenophidian snakes (Squamata: Serpentes). *PLoS ONE* 14 (5): e0216148. https://doi.org/10.1371/journal.pone.0216148

Zar J.H. 1999. *Biostatistical Analysis*. Prentice-Hall, Englewood Cliffs, USA.

Appendix 1. Material examined. Coordinates are given in SIRGAS2000 (Sistema de Referencia Geocêntrico para as Américas, 2000) datum. Specimens marked with an asterisk (*) could not be found in their respective collections during the time of writing (15 October 2021), and are likely to be either missing or were destroyed during the Butantan Institute Fire in 2010.

Apostolepis aff. *niceforoi* Amaral, 1935 (n = 1). BRAZIL: Roraima: Caracaraí, Vila de Caicubi, Rio Jufari, 1.797409ºS, 61.143789ºW (MZUSP 19625).

Apostolepis albicollaris Lema, 2002 (n = 24). BRAZIL: Distrito Federal: Brasília, 15.775247ºS, 47.922950ºW (USNM 148789, 148790, MCP 8354, 8355 (holotype), 8565, 9188, IBSP 55142*, 55143*, 62498*, 63913*, 20617*, 20618*, 26760*, 63916*, 63917*, CHUNB 23782, 23783); Goiás: Alexânia, 16.073833ºS, 48.500497ºW (IBSP 63916), Ipameri, 17.72194ºS, 48.15972ºW (IBSP 1822*, 92626, 92627), Minaçu, Cana Brava UHE, 13.510069ºS, 48.209950ºW (MCP 15219 (holotype of *Apostolepis cerradoensis*), IBSP 26712*, AMNH-R 144575).

Apostolepis ambiniger (Peters, 1869) (n = 21). PARAGUAY: Unknown locality (ZMB 6450 (holotype of *Rhynchonyx ambiniger*), MNRJ 760, 761, 762, NMW 13807, USNM 73458); Amambay: Pedro Juan Caballero, 22.556997ºS, 55.727736ºW (MCZ 47002); Cordillera: "Bei" (Eng: "in") Altos, 25.264344ºS, 57.254242ºW (NMW 20721); Departamento Central: Unknown locality (MVZ 110991), Areguá, 25.303760ºS, 57.411182ºW (MHNP 5163), Asuncíon, 25.272547ºS, 57.584233ºW (ZMB 28729, BMNH 1930.11.27.228, 1834.3.14.70, 1834.3.14.71, 1834.3.14.72, 1834.3.14.73, SMF 20340), Villa Hayes, Asuncíon, 25.272550ºS, 57.584240ºW (ZMB 32144), San Lorenzo, 25.353124ºS, 57.505877ºW (MHNP 3493), Trinidad, 27.128686ºS, 55.706528ºW (UMMZ 108809); Presidente Hayes: Chacoí, 25.248977ºS, 57.645968ºW (ZMB 32144).

Apostolepis arenaria Rodrigues, 1993 (n = 5). BRAZIL: Bahia: Originally given as "Alagoado", corrected to Casa Nova municipality, 9.161121ºS, 40.983073ºW (MZUSP 10027, 10028, 10029, 10030, 10289).

Apostolepis assimilis (Reinhardt, 1861) (n = 139). BRAZIL: Bahia: Barreiras, 12.143650ºS, 45.003059ºW (UMMZ 20411), previously reported as from "Trindad, Paraguay"herein redetermined to be from "Unknown locality, Bahia" (UMMZ 108810); Distrito Federal: Brasília, 15.775247ºS, 47.922950ºW (CHUNB 24456, 24474, IBSP 20566, 28734, USNM 148790); Goiás: border with Tocantins, Ilha do Bananal, Santa Isabel, 11.080152ºS, 50.636316ºW (IBSP 12324), Jataí, 17.899968ºS, 51.730803ºS (MZUSP 3783), Mineiros, 17.558692ºS, 52.552554°S (IBSP 55495), Rio Verde, 17.787982ºS, 50.937775ºW (IBSP 10326, 12945, MZUSP 3194), Uruaçu, Cana Brava, 14.519870ºS, 49.150580ºW (IBSP 9154); Minas Gerais: Cabo Verde, 21.475110ºS, 46.397057ºW (IBSP 29448), Cambuí, 22.614916ºS, 46.056915ºW (IBSP 44222), Capão dos Porcos, Mariana, 20.365709ºS, 43.407326ºW (ZMUC 63806 (holotype), Caxambu, 21.98007ºS, 44.932633ºW (IBSP 816), Conceição dos Ouros, 22.412537ºS, 45.800055ºW (IBSP 33206), Entre Rios de Minas, 20.680355ºS, 44.089915ºW (FUNED 691), Gonçalves, 22.658901ºS, 45.856063ºW (IBSP 49666), Ibirité, 20.012663ºS, 44.081203ºW (FUNED 603), Itajubá, 22.434017ºS, 45.467651ºW (IBSP 9115, 9407, 9592), Itamonte, 22.284305ºS, 44.874096ºW (IBSP 22405), Itatiaiuçu, 20.204767ºS, 44.462560ºW (FUNED 510), Jaíba, 15.345628ºS, 43.686232ºW (FUNED 1465), Maria da Fé, 22.307992ºS, 45.378278ºW (IBSP 5597), Moeda, 20.330538ºS, 44.055868ºW (FUNED 02), Nova Lima, 20.004714ºS, 43.871471ºW (FUNED 550), Ouro Fino, 22.278276ºS, 46.374551ºW (IBSP 34306), Munhoz, 22.278276ºS, 46.374551ºW (IBSP 66376), Passa Quatro, 22.389193ºS, 44.972256ºW (IBSP 3264, 3274, 34306), Poços de Caldas, 21.812489ºS, 46.588499ºW (IBSP 45737, 23985, 14256), Pouso Alegre, 22.246732ºS, 45.927618ºW (IBSP 42162, 44597, 49942), Santa Rosa da Serra, 19.530423ºS, 45.967855ºW (IBSP 46088), Serra do Cipó, 19.370279ºS, 43.585560ºW (MZUSP 7595), Uberabinha, border with São Paulo, 20.016022ºS,

47.793120ºW (IBSP 888), Uberlândia, 19.133733ºS, 48.333231ºW (IBSP 3841, 3845, 6388, 3841), Vespasiano, 19.734960ºS, 43.939672ºW (FUNED 04); Mato Grosso do Sul: Amambaí, 23.111955ºS, 55.230187ºW (IBSP 41163), Campo Grande, 20.494551ºS, 54.610826ºW (IBSP 42978, 57222, MHNCI 6719, MZUSP 10155), Nova Andradina, 22.002500ºS, 53.491960ºW (IBSP 27489, 27489), Paranaíba, 19.671986ºS, 51.191663ºW (IBSP 45615), Ponta Porã, 22.512971ºS, 55.713606ºW (IBSP 44065); Mato Grosso: Buriti, 17.973681ºS, 53.554398ºW (IBSP 5346), Cuiabá, 15.426759ºS, 55.943251ºW (MNRJ 2031); Paraná: Londrina, 23.322525ºS, 51.176065ºW (IBSP 37462, 40008); Santa Catarina: Florianópolis (previously BGSS 5344, currently ZFMK 102120, locality possibly in error, see Entiauspe-Neto et al. 2020d); São Paulo: Araçariguama, 23.441586ºS, 47.069288ºW (IBSP 83132), Barueri, 23.515768ºS, 46.882181ºW (IBSP 23206), Bauru, 22.327818ºS, 49.107726ºW (MHNCI 4790), Cabreúva, 23.316678ºS, 47.082624ºW (IBSP 26565), Caieiras, 23.374820ºS, 46.735134ºW (IBSP 40320), Caixa d'Água, coordinates unknown (IBSP 6659), Carapicuíba, 23.540539ºS, 46.846607ºW (IBSP 87769, 82260), Cajamar, 23.348228ºS, 46.877875ºW (IBSP 30408, 87083, 3186), Campo Largo, 25.463235ºS, 49.537514ºW (IBSP 4498), Campo Limpo, 23.635070ºS, 46.754990ºW (IBSP 6532), Campos do Jordão, 22.735380ºS, 45.583899ºW (IBSP 26796, UMMZ 204112), Carapicuíba, 23.54919ºS, 46.84454ºW (IBSP 72970), Cotia, 23.636020ºS, 46.956576ºW (IBSP 24588), Ibiúna, 23.662839ºS, 47.213951ºW (IBSP 32672, 79312, 78900), Itapevi, 23.554159ºS, 46.978074ºW (IBSP 30436, 86908, 79489), Itatiba, 22.993786ºS, 46.824113ºW (IBSP 5703), Itu, 23.297557ºS, 47.301031ºW (IBSP 4180, 6606, 82230, MHNCI 6969, MZUSP 4180, 6606), Jaguara, 23.512151ºS, 46.742029ºW (IBSP 70356), Jandira, 23.543093ºS, 46.900625ºW (IBSP 31694, 40493), Jarinu, 23.116928ºS, 46.716730ºW (IBSP 30019), Jundiaí, 23.203436ºS, 46.939945ºW (IBSP 16688), Mairinque, 23.539455ºS, 47.185860ºW (IBSP 41065, 89049), Osasco, 23.540895ºS, 46.795779ºW (IBSP 23889, 40480, 6141, 62362, 78442, MCP 64), Pirituba, 23.474910ºS, 46.743881ºW (IBSP 70351, 78948), "Rio Grande", coordinates unknown (IBSP 40008), Santana de Parnaíba, 23.457582ºS, 46.918621ºW (IBSP 61761, 81066), São Caetano do Sul, 23.626138ºS, 46.565080ºW (IBSP 81238), São Paulo, 23.534933ºS, 46.609078ºW (IBSP 318, 348, 6401, 6558, 8040, 8945, 21993, 22221, 24180, 24548, 24873, 27598, 30153, 30586, 31716, 32441, 33316, 84949, 78948), São Roque, 23.528545ºS, 47.141170ºW (IBSP 23548, 78641, 79658, MHNCI 4495, 6970), Sorocaba, 23.481770ºS, 47.455341ºW (IBSP 15760, 40008).

Apostolepis cearensis Gomes, 1915 (n = 146). BRAZIL: Alagoas: Piranhas, 9.607967ºS, 37.768092ºW (CHUFS 3217, 3365, MUFAL 1315); Bahia: Brumado, 14.207125ºS, 41.675605ºW (IBSP 33651, 33685), Camaçari, 12.706750ºS, 38.331172ºW (MZUEFS 371), Capim Grosso, 11.381030ºS, 40.010385ºW (MZUEFS 294), Feira de Santana, 12.223937ºS, 38.990827ºW (MZUEFS 12, 19, 70, 71, 74, 86, 130, 162, 166, 203, 277, 310, 315, 429, 434, 463, 464, 505, 515, 615, 624, 637, 669, 672, 689, 771, 804, 836, 841, 895, 927, 1007, 1040, 1053, 1067, 1069, 1070, 1071, 1077, 1080, 1110, 1146, 1157, 1158, 1195, 1196, 1208, 1209, 1210, 1236, 1240, 1241, 1244, 1260, 1302, 1310, 1313, 1369, 1377, 1405, 1445, 1446, 1477, 1478, 1479, 1499, 1539, 1559, 1570, 1587, 1604, 1611, 1622, 1629, 1645, 1673, 1674), Poções, 14.526737ºS, 40.366499ºW (MZUFBA 1595, 1796, 1805, 1813, 1826, 1827), São Gonçalo dos Campos, 12.435848ºS, 38.952627ºW (MZUEFS 73, 825), Jaguarari, 10.258500ºS, 40.194672ºW (IBSP 26203); Ceará: Aquiraz, 3.910332ºS, 38.383874ºW (CHUFC 1185), Beberibe, 4.183106ºS, 38.131271ºW (CHUFC 1628), Crateús, 5.174963ºS, 40.675624ºW (CHUFC 2238), Crato, 7.244635ºS, 39.448914ºW (IBSP 20385), Fortaleza, 3.76337ºS, 38.527876ºW (CHUFC 208, 826, 1240, 1242, 1243, 1524, 1525, 1526, 1527, 1528, 1529, 1531, 1539, 1620, 1621, 1622, 1623, 1623, 1624, 1625, 1626, 1627, 1629, 2001, 2236, 2287, 2243, 2633, IBSP 20020, 40262, 55318, 18219, 18220), Icó, 6.400202ºS, 38.860449ºW (IBSP 12106), Juazeiro do Norte, 7.228342ºS, 39.314310ºW (IBSP 20164), Limoeiro do Norte, 5.140528ºS, 38.071232ºW (IBSP 12775), Maranguape, 3.889587ºS, 38.678660ºW (CHUFC 2235), Quixadá, 4.969875ºS, 39.017092ºW (CHUFC 1221), São Benedito, 4.045633ºS, 40.865595ºW (CHUFC 2114, 2147), Tianguá, 3.727411ºS, 40.997394ºW (IBSP 77109), Ubajara, 3.865421ºS, 40.980188ºW (IBSP 75855, 77101), Viçosa do Ceará, 3.566272ºS, 41.110413ºW (IBSP 77509); Paraíba: Cabaceiras, 7.490668ºS, 36.288036ºW (MZUSP 9013), Campina Grande, 7.230571ºS, 35.892641ºW

(IBSP 9050), Lagoa de Dentro, 6.673537ºS, 35.377482ºW (MNRJ 17055); Piauí: Teresina, 5.052687ºS, 42.764437ºW (IBSP 49743), Redenção do Gurguéia, 9.488261ºS, 44.583311ºW (IBSP 80942).

Apostolepis christineae Lema, 2002 (n = 2). BOLIVIA: Santa Cruz: Puerto Suarez, German Busch, 18.970739ºS, 57.816239ºW (BMNH 1907.10.31.62). BRAZIL: Mato Grosso: Cáceres, 16.076427ºS, 57.675286ºW (MCP 12515 (holotype)).

Apostolepis dimidiata (Jan, 1862) (n = 11). BRAZIL: Mato Grosso: Unknown locality (AMNH 62192); São Paulo: Unknown locality (AMNH 7245, 102252, FMNH 69934, MCZ 27661, USNM 76369, 76370, ZUEC 936, 2277, 0884, 947).

Apostolepis dorbignyi (Schlegel, 1837) (n = 2). "AMÉRIQUE MÉRIDIONALE": Unknown locality (MNHN 3664 (holotype)). BOLIVIA: Tarija (MZUT 963).

Apostolepis flavotorquata (Duméril, Bibron & Duméril, 1854) (n = 6). BRAZIL: Bahia: Unknown locality (UMMZ 108808); Mato Grosso: Unknown locality (AMNH 93559, 935690, 93561, SMS voucher unavailable); Distrito Federal: Brasília, 15.775247ºS, 47.922950ºW (IBSP 81159).

Apostolepis gaboi Rodrigues, 1993 (n = 34). BRAZIL: Bahia: Ibiraba, Barra, 10.787131ºS, 42.823709ºW (MZUFBA 1673, 1674, 1675, 1676, 1677, 1678, 1679, 1680, 1681, 1682, 1683, 1684, 1685, 1686, 1687, 1688, 1689, 1690, 1691, 1692, 1693, 1694, 1695, 1696, 1697, 1698, 1699, 1700, 1701, 1702, 1702, 1704), Icatú Barra, 10.787140ºS, 42.823790ºW (MZUEFS 981), Queimadas, 11.042418ºS, 39.699621ºW (MZUSP 10290).

Apostolepis goiasensis Prado, 1942 (n = 4). BRAZIL: Goiás: Rio Verde, 17.79720ºS, 50.917500ºW (IBSP 10260* (holotype); Minas Gerais: Três Lagoas, 20.788371ºS, 51.706916ºW (CHFURG 1344, IBSP 90238, 90239).

Apostolepis intermedia Koslowsky, 1898 (n = 3). BRAZIL: Minas Gerais: Três Lagoas, 20.788371ºS, 51.706916ºW (IBSP 90237). PARAGUAY: San Pedro: Laguna Blanca, 23.808604ºS, 56.283731ºW (MHNP 11533, 11636).

Apostolepis kikoi Santos, Entiauspe-Neto, Silva-Araújo, Souza, Lema, Strüssmann & Albuquerque, 2018 (n = 5). BRAZIL: Mato Grosso: APM Manso, Chapada dos Guimarães, 15.090012ºS, 55.712671ºW (MCP 11372, 12096 (holotype), 14524, 14525, UFMTR 1933 (paratypes)).

Apostolepis lineata Cope, 1887 (n = 1). BRAZIL: Mato Grosso: Chapada dos Guimarães, 15.090012ºS, 55.712671ºW (ANSP 11211 (syntype)).

Apostolepis longicaudata Gomes, 1921 (n = 1). BRAZIL: Tocantins: Estação Ecológica Serra Geral, 10.856603ºS, 46.696670ºW (MZUSP 14122).

Apostolepis multicincta Harvey, 1999 (n = 5). BOLIVIA: Santa Cruz: San Juan, 20.900597ºS, 67.765903ºW (ZFMK 66375 (paratype)), Florida, 19.450080ºS, 65.450257ºW (ZFMK 75025, 75026), Santa Cruz, 17.792752ºS, 63.162745ºW (MNKR 729 (holotype), 878 (paratype)).

Apostolepis nelsonjorgei Lema & Renner, 2004 (n = 2). BRAZIL: Goiás: Campinaçú, 13.787851ºS, 48.571293ºW (MZUSP 20636); Tocantins: Estação Ecológica Serra Geral, 10.856603ºS, 46.696670ºW (MZUSP 17615).

Apostolepis niceforoi Amaral, 1935 (n = 1). COLOMBIA: Caquetá: Florencia, -1.614836ºS, 75.608047ºW (ICN 10422).

Apostolepis nigrolineata (Peters, 1869) (n = 207). SOUTH AMERICA (ZMB 6447 (holotype)). BRAZIL: Unknown locality (BMNH 1946.1.9.82 (holotype of *Apostolepis pymi*)); Maranhão: Paruá, BR 316, 2.509304ºS, 45.785033ºW (MPEG 10835, 13641, 14352); Maranhão/Pará border: BR 316, km 74, unknown coordinates (MPEG 1064, 1084, 3581, 8192, 10851); Mato Grosso: Paranaita, 9.673178ºS, 56.473624ºW (MZUSP 22344); Pará: Acará, 1.954775ºS, 48.198985ºW (MPEG 10939), Ananindeua, 1.363090ºS, 48.383168ºW (MPEG 6943, 9459), Apeú, 1.300842ºS, 47.988234ºW (MPEG 586, 587, 696, 1174, 1476, 1479, 2657, 2666, 3331, 3332, 3334, 3335, 5718, 6916, 6919, MCP 11317), Augusto Correa, 1.096654ºS, 46.524358ºW (MPEG 3905, 3954, 5399, 6712, 6713, 6721, 6724, 6737, 8999, 9937, 10764, 12450, 13074), Baião, 2.791305ºS, 49.669744ºW (MPEG 1596, 1600, 1605, 1891, 1897, 2101, 2422, 2423, 2560, 2822, 2826, 2864, 2866, 3386, 3387, 3389, 3390, 3448, 3949, 3950, 3951, 4086, 4094, 4801, 4802, 4807, 4808, 4811, 4813, 4817, 4828, 4858, 8187), Belém, 1.255141ºS, 48.457572ºW (IBSP 3033, 3034, 54152, KU 127256, 127257, 140153, 140154, MPEG 12769, 12770, 12771), Benevides, Genipaula Road, Pratinha, 1.363915ºS, 48.253507ºW (MPEG 7570, 8399, 8615, 8631, 12575, 14285, 15476), Cachoeira do Piriá, 1.760485ºS, 46.546425ºW (MPEG 2174, 2970, 5160, 7821, 7827, 9546, 9558, 9818, 9829, 11486, 11488, 11933, 11937, 12882, 12883, 15060, 15063, 15863), Castanhal, 1.289674ºS, 47.932947ºW (MPEG 5878, 7163, 7173, 10912, 10913, 11794, 12693), Gurupá, 1.000374ºS, 51.464640ºW (MPEG 16324), IgarapéAçu, 1.137108ºS, 47.619212ºW (MPEG 868, 869, 870, 871, 910, 912, 913, 924, 925), Inhangabi, 1.431096ºS, 47.910219ºW (MPEG 1464, 1568, 1571), Marabá, 5.345396ºS, 49.118178ºW (MPEG 17304), Ilha de Outeiro, 1.259871ºS, 48.445750ºW (MCP 10718), Ourém, 1.551101ºS, 47.117504ºW (MPEG 4224, 5004, 5005, 5012, 7016, 7019), Santa Bárbara do Pará, 1.189924ºS, 48.257630ºW (MPEG 1855, 2608, 3952), Santarém, 2.445930ºS, 54.730186ºW (MPEG 8011), Santarém Novo, 0.908698ºS, 47.348546ºW (MPEG 1841, 1977, 3251, 4154, 4796, 7081), Santo Antônio do Tauá, 1.081319ºS, 48.161660ºW (MPEG 1000, 1453, 1872, 1873, 1879, 2375, 2376, 2643, 3306, 3940, 4718, 4720, 4721, 4723, 4730, 6958, 7557), Serra dos Carajás, 6.277626ºS, 50.581624ºW (MZUFV 1071), Serra de Kukoinhokren (herein inferred as Ourilandia do Norte), 6.753257ºS, 51.0794844ºW (MZUSP 1068485), Uruá, 4.544668ºS, 56.311443ºW (IBSP 7285, MZUSP 7287), Utinga, unknown coordinates (KU 128094), Viseu, 1.575437ºS, 46.570213ºW (MPEG 1735, 1787, 2292, 2293, 2323, 2349, 3714, 3953, 4458, 5239, 5249, 5320, 5321, 5324, 5325, 5327, 5329, 6633, 7291, 7325, 7338, 7701, 8959, 10010, 10884, 10886, 10887, 11267, 11268, 13260, 15126, 15127, 17279, 314243); Rondônia: Machadinho do Oeste, 9.349686ºS, 61.981843ºW (MZUSP 21888); Mato Grosso: Pontes e Lacerda, 15.232549ºS, 59.333494ºW (MPEG 2500).

Apostolepis nigroterminata Boulenger, 1896 [sensu lato] (n = 15). BOLIVIA: Unknown locality (USNM 280371); Santa Cruz: Unknown locality (BMNH 1927.8.1.180, 1927.8.1.181, 1927.8.1.182, CM 2909, MNKR 472, 942, UMMZ 60773, 67962, 67963, UTA 44687). BRAZIL: Acre: Km-80 da BR-317, Fazenda da Patroa, near Boca do Acre, -9.604718ºS, -67.320209ºW (UFAC 383); Mato Grosso: Comodoro, 13.657177ºS, 59.795470ºW (MPEG 26500), Vila Bela da Santíssima Trindade, 15.005081ºS, 59.948396ºW (MZUSP 6408). PERU: Cayaria (herein considered as Pucallpa), 8.360497ºS, 74.585841ºW (BMNH 1946.1.9.77 (holotype)).

Apostolepis quinquelineata Boulenger, 1896 (n = 2). GUYANA: Georgetown, -6.797002ºS, 58.156512ºW (BMNH 89.9.30.12 (holotype)). BRAZIL: Amazonas: Presidente Figueiredo, 2.031079ºS, 60.025275ºW (INPAH 31440).

Apostolepis quirogai Giraudo & Scrocchi, 1998 (n = 1). BRAZIL: Rio Grande do Sul: Santo Ângelo, Campus URI, 28.277008ºS, 54.270656ºW (MCP 12185).

Apostolepis rondoni Amaral, 1925 (n = 2). BRAZIL: Rondônia: Porto Velho, 8.758575ºS, 63.883062ºW (UFRO-H 228, 229).

Apostolepis sanctaeritae Werner, 1924 (n = 33). BRAZIL: Bahia: Unknown locality (MCP 8442), Cocos, 14.181859ºS, 44.537064ºW (IBSP 61525, CHUNB 23715, 51360), Correntina, 13.571514ºS, 45.303100ºW (CHUNB 39079), Santa Rita de Cássia, Ibipetuba, 10.866069ºS, 44.610886ºW (NMW 23452 (holotype), MZUFBA 728 (topotype)); Distrito Federal: Brasília, 15.775247ºS, 47.922950ºW (IBSP 49363); Goiás: Unknown locality (IBSP 15723), Minaçu, 13.510069ºS, 48.209950ºW (IBSP 40478, AMNH-R 144574), São Domingos, 13.401192ºS, 46.322214ºW (IBSP 62593, 67392); Mato Grosso: Nova Xavantina, 14.662802ºS, 52.362981ºW (MCP 8002), Ribeirão Cascalheira, 12.939072ºS, 51.828372ºS (MCP 19481), São Félix do Araguaia, 11.617427ºS, 50.666608ºW (IBSP 15723); Minas Gerais: Betim, 19.925915ºS, 44.222527ºW (FUNED 03), Curvelo, 18.762770ºS, 44.440999ºW (IBSP 22410), Pirapora, 17.353695ºS, 44.889140ºW (MPEG 18347), Serra do Cipó, 19.370279ºS, 43.585560ºW (MZUSP 7595), Três Marias, 18.218011ºS, 45.239204ºW (FUNED, Without voucher), Vazante, 17.989087ºS, 46.899214ºW (IBSP 48041); Tocantins: Gurupi, 11.729458ºS, 49.074318ºW (MZUSP 8007), Lajeado, 9.839862ºS, 48.321855ºW (IBSP 64533, 64534, 65571, 65680, 65681), Palmas, 10.283001ºS, 48.342440ºW (IBSP 65267* (holotype of *Apostolepis ammodites*)), Porto Nacional, 10.683005ºS, 48.377269ºW (IBSP 65682, 65683, 66166), Santa Isabel, 11.384446ºS, 48.073970ºW (IBSP 12324).

Apostolepis tenuis Ruthven, 1927 (n = 2). BOLIVIA: Beni: Guayaramirim, 10.827529ºS, 65.363502ºW (USNM 123973); Santa Cruz: Buena Vista, Ichilo, 16.888852ºS, 64.189732ºW (UMMZ 64436 (holotype)).

Apostolepis thalesdelemai Borges-Nojosa, Lima, Bezerra & James, 2016 (n = 35). BRAZIL: Ceará: Guaramiranga, 4.261648ºS, 38.932367ºW (CHUFC 1950, 2067, 2353, 2371), Ibiapina, 3.925965ºS, 40.888903ºW (CHUFC 2337, 2340, 2342, 2343, 2351, 2437), Maranguape, 4.008095ºS, 38.818735ºW (CHUFC 2102, 2208, 2212, 2213, 2218, 2339, 2347, IBSP 80734), Pacoti, 4.226994ºS, 38.921911ºW (CHUFC 2344, 2346, 2463, 2731, 2841), São Benedito, 4.047003ºS, 40.866281ºW (CHUFC 2338), Ubajara, 3.859255ºS, 40.926629ºW (CHUFC 1349, 2085, 2110, 2137, 2154, 2341, 2350, 2769, 2954, IBSP 80735, ZUEC 3384).

Apostolepis vittata (Cope, 1887) (n = 4). BRAZIL: Mato Grosso: Chapada dos Guimarães, 15.090012ºS, 55.712671ºW (ANSP 11293 (holotype of *Rhynchonyx ambiniger vittatus)*, CHUNB 30656), Parque Nacional Chapada dos Guimarães, 15.090012ºS, 55.712671ºW (UFMTR 12259), Rio da Casca, 15.359774ºS, 55.458283ºW (MCP 13283).

Parapostolepis polylepis (Amaral, 1922) (n = 1). BRAZIL: Piauí: Gilbués, 9.825100ºS, 45.343900ºW (IBSP 90724).

Supplementary material

Supplemental Material from: "Unveiling an enigma from the Cerrado: taxonomic revision of two sympatric *Apostolepis* Cope, 1862 species (Dipsadidae: Elapomorphini) from Central Brazil". Figshare Dataset. Available from https://doi.org/10.6084/m9.figshare.16985383.v1

Supplementary Table 1. Morphological data for *Apostolepis* in the Brazilian Cerrado (.xls).

Supplementary Table 2. Geographic distribution data for *Apostolepis albicollaris* in the Brazilian Cerrado (.xls).

Supplementary Table 3. Accession number for gene fragments used in this study (.xls).

Supplementary Table 4. Patristic distances between the genera *Apostolepis*, *Phalotris*, *Elapomorphus*, *Taeniophallus*, *Tomodon*, *Thamnodynastes*, *Sordellina*, and *Philodryas*, as inferred in this study (.txt).

Supplementary File 1. *12S* gene alignment (.fasta).

Supplementary File 2. MEGA output for uncorrelated *p*-distances of *12S* alignment (.txt).

Supplementary File 3. *CMOS* gene alignment (.fasta).

Supplementary File 4. MEGA output for uncorrelated *p*-distances of *CMOS* alignment (.txt).

Supplementary File 5. Concatenated alignment of mtDNA (*12S*, *16S*, *CYTB*, *ND2*, *ND4*) and nuDNA (*BDNF*, *CMOS*, *NT3*, *RAG1*) genes (.fasta).

Supplementary File 6. Output maximum likelihood RAxML pruned tree file (.newick).

Supplementary File 7. Output Bayesian inference MrBayes pruned tree file (.newick).